Metabolic control of type 2 innate lymphoid cells plasticity toward protective type 1-like cells during *Mycobacterium tuberculosis* infection

Dan Corral[1#], Alison Charton[1], Maria Z Krauss[2], Eve Blanquart[3], Florence Levillain[1], Emma Lefrançais[1], Jean-Philippe Girard[1], Gérard Eberl[4], Yannick Poquet[1], Jean-Charles Guéry[3], Rafael J Arguello[5], Matthew R Hepworth[2], Olivier Neyrolles[1,6] and Denis Hudrisier[1,6#]

[1]Institut de Pharmacologie et Biologie Structurale, IPBS, Université de Toulouse, CNRS, UPS, Toulouse, France

[2]Lydia Becker Institute of Immunology and Inflammation, Division of Infection, Immunity and Respiratory Medicine, School of Biological Sciences, Faculty of Biology, Medicine and Health, Manchester Academic Health Science Centre, University of Manchester, Manchester, M13 9PL, UK

[3]Centre de Physiopathologie de Toulouse Purpan (CPTP), Université de Toulouse, INSERM, CNRS, UPS, Toulouse, France

[4]Institut Pasteur, Microenvironment & Immunity Unit, 75724 Paris, France ; INSERM U1224, 75724 Paris, France

[5]Aix Marseille Univ, CNRS, INSERM, CIML, Centre d'Immunologie de Marseille-Luminy, Marseille, France

[6]These authors contributed equally: Olivier Neyrolles, Denis Hudrisier

[#]Corresponding authors: dan.corral@ipbs.fr; denis.hudrisier@ipbs.fr

Abstract

Tissue-resident innate lymphoid cells (ILCs) regulate tissue homeostasis and protect against pathogens at mucosal surfaces and are key players at the interface of innate and adaptive immunity. How ILCs adapt their phenotype and function to environmental cues in their tissue of residence remains to be fully understood. Here we show that *Mycobacterium tuberculosis* infection alters the biology of lung ILCs and, in particular, induces the emergence of a non-classical, protective, interferon-γ-producing ILC1-like population. Adoptive transfer, fate-mapping and *in vitro* differentiation experiments revealed that ILC1-like cells originate from immature ILC2 rather than from mature ILC2. This plasticity is controlled by type 1 cytokines and a glycolytic program involving the transcription factor HIF1α. Collectively, our data reveal how tissue-resident ILCs adapt to their inflammatory and metabolic environment to undergo phenotypic and functional changes toward a pathogen-adapted immune response.

37 ## Introduction

38

39 Innate lymphoid cells (ILCs) are a population of tissue-resident cells of lymphoid
40 origin that play a key part in both tissue homeostasis and immunity. ILCs are
41 subdivided into three distinct populations based on their expression of cytokines and
42 specific transcription factors. ILC1 depend on T-bet and produce interferon (IFN)-γ,
43 ILC2 depend on GATA3 and produce interleukin (IL)-5 and IL-13, and ILC3 depend on
44 RORγt and produce IL-17A and IL-22[1,2]. Based on these properties, group 1, 2 and 3
45 ILCs are commonly presented as the innate counterparts of T helper type 1 (Th1), Th2
46 and Th17 cells, contributing to type 1, 2 and 3 immune responses, respectively.
47 The regulome of ILCs evolves progressively during the development of each
48 population to reach a state in which key loci relative to that population's specific
49 functions are primed[3]. Yet, several elements controlling cytokine expression or loci
50 encoding lineage-determining transcription factors remain broadly accessible in all ILC
51 subsets[3]. This feature contributes to the remarkable ability of ILCs to dynamically adapt
52 to physiological or pathological alterations in their tissue of residence and to adopt new
53 phenotypic and functional profiles. Thus, the various populations of tissue-resident
54 ILCs can promptly sense and adapt to environmental changes[1, 4] but how they do so
55 only begins to be explored.
56 In the murine model and in the human pathology of *Mycobacterium tuberculosis*
57 (*Mtb*) infection, prolonged proinflammatory responses are associated with oxidative
58 stress, which favors tissue destruction and triggers a tissue remodeling program. *Mtb*
59 infection is also associated with metabolic changes in the lungs, involving the utilization
60 of aerobic glycolysis primarily instead of oxidative phosphorylation (OXPHOS) in
61 mitochondria (Warburg effect)[5,6]. At the cytokine level, the lungs at steady-state mostly
62 host resting ILC2, which, together with alveolar macrophages, imprint a type 2-oriented
63 environment to the tissue[7,8]. *Mtb* infection of the lung triggers dramatic changes leading
64 to the development of type 1 immunity that is mediated by IFN-γ and associated with
65 protection[9]. While IFN-γ production by $CD4^+$ T lymphocytes in *Mtb* infection[109] has
66 been evidenced for a long time, a recent study in humans provided compelling
67 evidence that other cell types, including ILC1 and ILC2, can contribute to the
68 production of this key cytokine[11].

69 Here, using the murine model of *Mtb* infection, we explored how lung ILCs respond
70 to chronic pulmonary infection and, in particular, how the major ILC subset in mouse
71 lungs ILC2 adapt to the type 1 inflammation during infection.
72

73 ## Results

74 **ILC1-like cells emerge in the lungs of *Mtb*-infected mice independent of T and**
75 **B cells**

76 We determined the dynamics and activation of ILC subsets in C57BL/6 mice
77 infected with H37Rv, a laboratory adapted *Mtb* strain. At steady-state, *bona fide* lung
78 ILCs were defined as a population that did not express lineage markers (CD3, CD4,
79 CD8, TCRβ, TCRαδ, CD49b, CD11b, CD11c, B220, CD19, F4/80, GR-1, TER119,
80 FcεR1a) but highly expressed CD90.2 and CD45.2 (Fig. 1a). ILC2, which represent
81 the major ILC population in the mouse lung, were identified after exclusion of ILC1
82 (NK1.1^{+}) and ILC3 (RORγt^{+}) cells. We observed significant heterogeneity among ILC2
83 at steady-state, with a subset expressing IL-18Rα that expressed ILC2 markers
84 GATA3, ST2, Arg1, and IL-5 at lower levels than in ILC2 cells not expressing IL-18Rα
85 (Fig. 1a and Supplementary Fig. 1a-d). Strikingly, during *Mtb* infection, IL-18Rα-
86 expressing ILC2 markedly increased and, importantly, an ILC population expressing
87 both IL-18Rα and T-bet emerged (Fig. 1a).

88 Further phenotypical analysis revealed that the ILC subset co-expressing IL-18Rα
89 and T-bet displayed little to no classical ILC2 markers GATA3, ST2, Arg1 and IL-5 (Fig.
90 1a, b and Supplementary Fig. 1e-g) or the ILC3 marker IL-17A (Fig. 1a and c). Like
91 ILC1, this subset expressed T-bet, CD49a and CD226 and produced IFN-γ (Fig. 1a
92 and d; Supplementary Fig. h-j). However, unlike ILC1 or NK cells, these cells did not
93 express NK1.1 (gated on NK1.1 negative ILCs), NKp46 or Eomes (Fig. 1a and
94 Supplementary Fig. 1k). We therefore named this new subset as ILC1-like cells. In
95 order to better decipher the heterogeneity of ILCs during *Mtb* infection, we used an
96 unsupervised flow cytometry approach. This allowed us to clearly identify the expected
97 presence and abundance of typical ILC subsets in uninfected animals and, more
98 importantly, the emergence of the ILC1-like subset during *Mtb* infection (Fig. 1e).

99 While ILC1, ILC3, and IL-18Rα^+ ILC2 increased following a similar kinetic upon *Mtb*
100 infection (Fig. 1f, g, h), IL-18Rα^- ILC2 progressively decreased (Fig. 1i). ILC1-like cells
101 became detectable after 21 days of infection and dramatically expanded in the
102 following weeks (Fig. 1j). The dynamics of these ILC populations was well reflected by
103 their index of proliferation, as revealed by Ki-67 staining (Supplementary Fig. 1l).
104 Interestingly, the emergence of ILC1-like cells was conserved in the C3HeB/FeJ
105 mouse, which is more sensitive to *Mtb*, both phenotypically and functionally
106 (Supplementary Fig. 1m-n).

107 Since the adaptive immune cells reach the site of infection starting from day 21 post-
108 *Mtb* infection[12] and therefore coincides with the detection of ILC1-like cells, we
109 determined if these two processes were linked. Interestingly, *Rag2*$^{-/-}$ mice lacking the
110 adaptive immunity presented an enhanced generation of ILC1-like cells compared to
111 wild-type mice, demonstrating that adaptive immunity is not necessary for the
112 generation of ILC1-like cells (Supplementary Fig. 1o).

113 Altogether, our data show that in the lung during *Mtb* infection, classical ILC1 and
114 ILC3 expand, IL-18Rα^- ILC2 contract and, most notably, a previously unidentified ILC1-
115 like cell population emerges, which contributes to IFN-γ production.

116

117 **Pulmonary ILC2 give rise to ILC1-like cells during *Mtb* infection**

118 ILCs have been reported to adapt their profile to environmental cues and ILCs with
119 characteristics of ILC1-like cells have been shown to emerge from various origins[13, 14].
120 Because we show, for the first time, the emergence of ILC1-like cells in the context of
121 *Mtb* infection and that ILC1-like cells were undetectable before the infection, we
122 hypothesized that ILC1-like cells could arise from pre-existing lung ILC2. To test this
123 hypothesis, we adoptively transferred total lung ILC2 purified based on ST2 positivity
124 regardless of their IL-18Rα expression into *Rag2*$^{-/-}$*Il2rg*$^{-/-}$ mice, which are devoid of T
125 cells, B cells, and NK/ILCs, one day before *Mtb* infection (Supplementary Fig. 2a and
126 b). Before transfer, we confirmed that purified ILC2 expressed GATA3 but not T-bet or
127 RORγt (Supplementary Fig. 2c) and noted that IL-18Rα expression was lost during *in*
128 *vitro* culture (Supplementary Fig. 2c). Confirming our hypothesis, transferred ILC2

129 strongly upregulated T-bet in infected, but not in non-infected, mice (Fig. 2a, b).
130 Furthermore, based on Ki67, T-bet^{high} cells represented the most proliferative
131 population among ILC2 (Fig. 2c). Importantly, higher amounts of IFN-γ were detected
132 in the lung of infected *Rag2*$^{-/-}$*Il2rg*$^{-/-}$ mice after ILC2 transfer (Fig. 2d), suggesting that
133 ILC1-like cells generated from ILC2 contribute to IFN-γ production.

134 Next, we determined if ILC1-like cells derive from mature, IL-5-producing, ILC2. For
135 this, we crossed IL-5$^{Cre\text{-}tdTomato}$ (Red5) mice with ROSA26-YFP mice to enable fate-
136 mapping mature ILC2[15] and confirmed that IL-5 was selectively expressed by ST2^{+}
137 ILC2 but not by IL-18Rα^{+} ILC at steady-state (Supplementary Fig. 2d). Surprisingly,
138 very few IL-18Rα^{+} ILC2 and ILC1-like cells expressed IL-5 and YFP after *Mtb* infection,
139 compared to IL-18Rα^{-} ILC2 (Fig. 2e, f). These results demonstrate for the first time that
140 mature ILC2 are not a major source for generating ILC1-like cells. In agreement with
141 this result, using a model of T-bet deficiency in IL-5^{+} cells (IL-5^{Cre}Tbx21$^{fl/fl}$ mice), we
142 found that ILC1-like cells remained present in spite of the absence of T-bet expression
143 in mature ILC2 (Supplementary Fig. 2e, f). Based on this set of results, we therefore
144 anticipated that ILC1-like cells most likely derived from immature ILC2.

145 We (Fig. 1 and Supplementary Fig. 1) and others[16,17] reported the presence of a
146 discrete subset of IL-18Rα^{+} ILC2 at steady-state harboring a less activated phenotype
147 compared to IL-18Rα^{-} ILC2 and ILC2 precursor (ILC2P). To assess if immature ILC2,
148 such as ILC2P from BM, have the potential to give rise to ILC1-like cells, we performed
149 an *in vitro* differentiation assay in the presence of type 1 or type 2 activating cytokines.
150 Because of the low numbers of ILC2P in the lungs, we purified them from the bone
151 marrow. We found that ILC2P acquired T-bet and IFN-γ expression, showing their
152 ability to engage in ILC1-like differentiation, only in the presence of type 1 cytokines
153 (Fig. 2g-j). In addition, we showed that the IL-18Rα^{+} ILC2 subset, unlike the IL-18Rα^{-}
154 ILC2 subset, shares similarities with bone marrow ILC2P, including the expression of
155 TCF-1 and PLZF, thus suggesting that this lung-resident subset forms a population of
156 immature ILC2 (Fig. 2k, l). Together, our results strongly suggest that immature rather
157 than mature ILC2 give rise to ILC1-like cells during *Mtb* infection.

158 **Type 1 and type 2 inflammation govern the generation of ILC1-like and mature**
159 **ILC2, respectively**

160 *Mtb* infection triggers the development of type 1 immunity [9] in the lung, which is
161 largely imprinted with a type 2 environment [7,8]. Therefore, we next investigated the
162 impact of type 1 and type 2 cytokines on the generation of ILC1-like cells. IL-12 is a
163 well-known cytokine initiating IFN-γ production by ILC1 and NK[18,19], which is
164 potentiated in the presence of IL-18[18,19]. Moreover, IL-18 complements IL-12's action
165 to establish a type 1 inflammatory environment during *Mtb* infection [9,20]. We
166 administered mice with IL-12 ± IL-18 intranasally for 1 week and found a decreased
167 ILC2 function, such as IL-5 production (Supplementary Fig 3a-c), in both mature and
168 immature ILC2 as well as an induced IFN-γ production in immature ILC2
169 (Supplementary Fig. 3c). Remarkably, administration of both IL-12 and IL-18 was
170 sufficient to induce the generation of IFN-γ -producing ILC1-like cells in the lungs (Fig.
171 3a-c). Thus, we could closely recapitulate the generation of ILC1-like cells observed
172 during *Mtb* infection with the simple administration of IL-12 and IL-18. IFN-γ is well-
173 known to repress ILC2 function[21,22], we therefore determined its role in the generation
174 of ILC1-like cells. IL-12+IL-18 administration led to a 3-fold reduction in the
175 differentiation of ILC1-like cells in *Stat1*$^{-/-}$ mice, which cannot signal through type 1 and
176 type 2 IFN, compared to in wild type mice (Fig. 3d, e). Similar results were obtained
177 upon blocking IFN-γ in WT mice (Fig. 3f). These results demonstrated a critical role
178 played by IFN-γ in driving ILC1-like differentiation.

179 IL-33, a well-known inducer of both mature and immature ILC2, had no impact on
180 the generation of ILC1-like cells but promoted their generation when combined with
181 IL12 and IL-18 (Fig. 3g and Supplementary Fig 3a). IL-33 alone clearly induced high
182 numbers of IL-18Rα^{+} ILC2 (Fig. 3g and Supplementary Fig 3a) but these cells
183 expressed IFN-γ only when IL-12+IL-18 were added (Supplementary Fig. 3a-d).
184 Interestingly, the combination of IL-12, IL-18, and IL-33 induced a mixed ILC1 and ILC2
185 phenotype characterized by the expression of both IL-5 and IFN-γ (Supplementary Fig.
186 3a-d). Because ST2 is expressed by various cell types, including ILC2, we also tested
187 Neuromedin U (NMU), whose receptor is solely present in bone marrow ILC2P and in
188 lung ILC2[23–25]. Similar to IL-33, NMU potentiated the generation of ILC1-like cells
189 induced by IL-12 and IL-18 (Fig. 3h).

190 These results strongly suggest that IL-18Rα^{+} ILC2 represent a highly adaptable
191 subset that retains the potential to differentiate into mature ILC2 or ILC1-like cells in

192 response to type 2 or type 1 cytokines, respectively, depending on the inflammatory
193 context.

194 **Metabolic environment dictates ILC2 plasticity through glucose availability**

195 Metabolism and metabolic reprogramming are key events in the development
196 and function as well as the adaptation to environmental cues of ILCs [26]. *Mtb* infection
197 is associated with inducing a Warburg effect in the lungs [5,6]. This observation prompted
198 us to explore if glycolysis impact on the cellular changes affecting ILC we report here.
199 To test this hypothesis, we first treated mice with 2-deoxyglucose (2-DG), a
200 glycolysis inhibitor, during *Mtb* infection (Fig. 4a). 2-DG administration marked
201 decreased both the percentage and the number of ILC1-like cells as well as diminished
202 the ability of ILC1-like cells to produce IFN-γ (Fig. 4b and c). Next, since glucose is
203 consumed in the lungs of *Mtb*-infected mice[6], we investigated if the modulation of
204 glucose availability in the lung environment could modulate ILC2 plasticity (Fig. 4d).
205 Glucose supplementation in the animals' drinking water greatly enhanced the
206 differentiation of ILC1-like cells (Fig. 4e) and augmented the percentage of IFN-
207 γ^+ ILC1-like cells (Fig. 4f). Interestingly, 2-DG or glucose supplementation had little to
208 no impact on other ILC subsets and their production of IFN-γ (Supplementary Fig. 4a-
209 b). There was a trend toward a decrease in NK cells upon 2-DG treatment and a
210 greater ability of these cells to produce IFN-γ upon glucose supplementation
211 (Supplementary Fig. 4c-f). Altogether, these results supported the hypothesis that the
212 metabolic environment controls ILC2 plasticity.

213 Arg1 was previously identified as a critical component of the metabolic programming
214 of lung ILC2, with its inhibition or genetic inactivation resulting in reduced aerobic
215 glycolysis[27]. Arg1 was highly expressed in both mature and immature ILC2 but not in
216 ILC1-like cells generated after *Mtb* infection or cytokine administration (Fig. 5a), which
217 prompted us to explore in more details the metabolic status of the ILC1-like cells. To
218 do this, we took advantage of the recently described SCENITH method[28], which allows
219 to functionally determine global metabolic dependencies and capacities at the single
220 cell level. SCENITH uses protein synthesis levels as a readout and is particularly
221 appropriate to analyze the metabolism of rare cells, such as ILCs. ILC1-like cells were
222 compared to control cells known to rely on a glycolytic metabolism (*e.g.* NK cells) and
223 to ILC2. IL-12+IL-18 administration increased and reduced protein synthesis levels in

224 NK cells and ILC2, respectively, as estimated by the staining for and the amount of
225 incorporated puromycin (Fig. 5b and c). ILC1-like cells presented the highest levels of
226 protein synthesis among all cells tested. These results are in accordance with the
227 activation status of these cells (Fig. 3). In addition, the analysis of protein synthesis in
228 the presence of inhibitors targeting different metabolic pathways allowed us to
229 assess glucose dependence, mitochondrial dependence and glycolytic capacity of the
230 cell types of interest (Fig. 5d-g). While IL-12+IL-18 administration did not affect the
231 glucose dependence of NK cells and ILC2 (Fig. 5e), it diminished mitochondrial
232 dependence while increased glycolytic capacity (Fig. 5f,g), a typical feature of the
233 Warburg effect[29]. The strong metabolic activity of ILC1-like cells (Fig. 5b,c) relied on
234 the glycolytic pathway similar to NK cells and ILC2 in IL12+IL-18 treated mice (Fig. 5e-
235 g). Surprisingly, the metabolic status of IL18Rα^+ ILC2 did not change upon IL-12+IL-
236 18 treatment, and therefore differed from that of NK and ILC1-like cells (Fig. 5e-g).
237 Finally, inhibition of glycolysis during *ex vivo* stimulation of total lung ILCs decreased
238 IFN-γ^+ ILCs (Fig. 5h), showing that IFN-γ production is glycolysis-dependent.

239 These results demonstrate that while the metabolic reprograming towards glycolysis
240 is observed in NK, ILC2 and ILC1-like cells, this metabolic profile is a hallmark of
241 activation for NK and ILC1-like cells and of inhibition for ILC2.

242

243 **Metabolic reprogramming involving HIF1α controls ILC2 plasticity**

244 Several studies suggested that the Warburg effect, a metabolic pathway that is at
245 work during *Mtb* infection[5,6], relied on the transcription factor hypoxia-inducible factor-
246 1 α (HIF1α) in a different context [30]. Interestingly, it was shown in a model of von
247 Hippel-Lindau (VHL) deficiency, where HIF1α is overexpressed, that ILC2
248 development was repressed through glycolysis induction[31]. IL-12+IL-18 administration
249 resulted in the activation of ILC1-like cells and the inhibition of ILC2 (Fig. 3) and
250 induced the glycolytic pathway (Fig. 5). This prompted us to investigate the
251 involvement of HIF1α in ILC2 plasticity toward ILC1-like.

252 HIF1α is regulated at both transcriptional and post-translational levels with O_2-
253 dependent and -independent mechanisms[30]. Because of technical limitations imposed

254 by the time necessary to process lungs in Biosafety Level 3 facility as well as by the
255 number of cells accessible, we could not use antibody-based approaches to measure
256 the HIF1α protein. Therefore, we measured the *Hif1a* mRNA level by flow cytometry in
257 non-infected *vs*. *Mtb*-infected mice. While *Hif1a* mRNA was poorly expressed in mature
258 ILC2 and NK cells in non-infected mice, its expression was strongly upregulated in
259 these cells during *Mtb* infection (Fig. 6a). In addition, *Hif1a* mRNA was expressed by
260 ILC1-like cells both at the expression level (Fig. 6a, left graph) and in the percentages
261 of expressing cells (Fig. 6a, right graph) compared to mature ILC2 from *Mtb*-infected
262 mice (Fig. 6a). Using this approach, we also confirmed that IFN-γ was well-induced in
263 NK cells and highly expressed by ILC1-like cells but was undetectable in ILC2 (Fig.
264 6b). Comparison of ILC1-like cells to mature and immature ILC2 during *Mtb* infection
265 showed that different percentages of these cells expressed *Il5* and *Ifng* mRNA (Fig.
266 6c-d), confirming the results of IL-5 and IFN-γ proteins (Fig. 1). The percentages of
267 cells expressing *Hif1a* mRNA was high and with no substantial differences among
268 these three cell subsets (Fig. 6e). Interestingly, the profile of *Ifng*, *Il5* and *Hif1a* mRNA
269 expression in ILC1-like cells and in mature and immature ILC2 in mice administered
270 with IL-12+IL-18 was similar to that in *Mtb*-infected animals (Supplementary Fig. 5a-
271 c), revealing that type 1 inflammation, including that induced by *Mtb* infection, drives
272 HIF1α expression in lung resident ILCs. Noteworthy, the expression of *Ifng* mRNA was
273 concomitant with *Hif1a* mRNA expression (Supplementary Fig. 5d). Moreover, the
274 generation of mitochondrial ROS (mtROS), an event tightly linked to HIF1α-
275 expression[32], was markedly upregulated in ILC1-like cells (Supplementary Fig. 5e),
276 suggesting that HIF1α protein could be differentially expressed between ILC1-like cells
277 and ILC2 although these subsets display comparable *Hif1a* mRNA levels. These
278 results support the notion that HIF1α is well-induced in ILC2 and ILC1-like cells,
279 suggesting that HIF1α might participate in ILC1-like differentiation through sustaining
280 glycolysis induction.

281 To further explore this hypothesis, we performed an *in vitro* assay using purified
282 ILC2 cultured in the presence of DMOG, which induces the stabilization of the HIF1α
283 protein[30] (Fig. 6f). DMOG-treated ILC2 reduced the expression of ILC2 markers
284 GATA3 and ST2 (Fig. 6g). Impressively, DMOG treatment alone was sufficient to
285 upregulate genes typically associated with an ILC1 phenotype, such as *Tbx21*, *Ifng*
286 and *Il18r1* (Fig. 6h). At the transcriptional level, DMOG treatment induced the

287 upregulation of genes implicated in the glycolytic pathway (Supplementary Fig.
288 5f). Accordingly, analysis of the global metabolic profile of ILC2 revealed that DMOG-
289 treated ILC2 harbored a glycolytic profile, while untreated ILC2 rather use
290 mitochondrial respiration (Fig. 6i-l).

291 Altogether, these results demonstrate that induction of HIF1α in lung ILC2 connects
292 glycolysis induction with the inhibition of their phenotype, which reminisces the
293 observation made in our *in vivo* models (Fig 1, 3, and 5), and favors, at the same time,
294 the acquisition of an ILC1-like profile.

295

296 **ILC1-like cells confer protection against *Mtb***

297 Next, we investigated whether BCG, the only available vaccine for TB, might impact
298 the population of lung-resident ILCs when delivered intranasally, a route providing a
299 better protection than the conventional subcutaneous route[33], prior to *Mtb* infection. As
300 expected, mucosal BCG vaccination induced protection upon *Mtb* challenge (Fig. 7a).
301 In vaccinated mice, protection correlated with an increase in T-bet expression in ILCs
302 (Fig. 7b). More importantly, although BCG vaccination had no impact on other ILC
303 subsets (Fig. 7c-g), higher numbers of ILC1-like cells were detected at 14 days post-
304 infection, a time when IFN-γ -producing ILC1-like cells were virtually absent from non-
305 vaccinated mice (Fig. 7e, h, i as well as Fig 1) but well-induced in vaccinated mice (Fig.
306 7e, h, i). Overall, BCG vaccination promotes ILC1-like cells in early stages of infection,
307 which could contribute to protection against *Mtb*.

308 We then addressed the protective role of ILC2 and ILC1-like cells against *Mtb* using
309 an adoptive transfer model. Transfer of purified lung ILC2 expanded *in vitro* did not
310 lead to a reduction in bacterial loads compared to non-transferred mice when analyzed
311 at 14 days post-infection. In sharp contrast, a statistically significant reduction in
312 bacterial load was observed in ILC2-transferred mice above control mice when
313 analyzed at day 21 post-infection (Fig. 7j). Interestingly, the increase in T-bet
314 expression was only observed after day 21, and not after day 14, strongly suggesting
315 that protection was rather due to ILC2 engaged in plasticity (Fig. 7k).

316 Finally, to assess the contribution of ILC2 plasticity to protection against *Mtb*, we
317 took advantage of the cytokine-based plasticity model (Fig. 2) to generate sufficient
318 numbers of ILC1-like cells for adoptive transfer. Remarkably, the transfer of as few as
319 10,000 ILC1-like cells resulted in a statistically significant reduction in bacterial load,
320 demonstrating for the first time the protective capacity of ILC1-like cells against the TB
321 bacillus (Fig. 7I).

322 **Discussion**

323 Here, we examined how *Mtb* infection impacts the biology of lung-resident ILCs in
324 the mouse model. We report that lung ILCs exhibit dramatic changes upon *Mtb*
325 infection, with ILC1 and ILC3 showing progressive expansion while mature ILC2, the
326 main ILC population in the lung, undergo contraction. Unexpectedly, an immature
327 subpopulation of ILC2 expressing IL-18Rα present in very low proportion at the steady
328 state progressively expand during infection. Even more strikingly, *Mtb* infection results
329 in the appearance of an ILC2 population exhibiting characteristics of ILC1 (ILC1-like
330 cells). Using a non-infection cytokine-dependent model, we found that immature ILC2
331 sense and adapt to their environment to strengthen the ILC2 response in a type 2
332 environment (administration of IL-33 or NMU) or to differentiate into IFN-γ-producing
333 ILC1-like cells in a type 1 environment (administration of IL-12 and IL-18). Importantly,
334 we found that type 1 immunity induces a glycolytic signature in both ILC2 and ILC1-
335 like cells but results in their inhibition and activation, respectively. Inhibition of
336 glycolysis or glucose supplementation *in vivo* revealed that both the generation and
337 function of ILC1-like cells critically depend on their metabolic environment.
338 Furthermore, stabilization of HIF1a in ILC2 is sufficient to trigger an ILC1-like signature
339 in these cells, suggesting a key role for HIF1a in ILC2-to-ILC1-like cell transition.
340 Finally, we report that ILC1-like cells are induced after BCG vaccination and exhibit a
341 protective potential against *Mtb* infection.

342 Recently, ILC3 were reported to mediate protection against *Mtb* through induction of
343 lung ectopic lymphoid follicles[34]. Although our results confirm the expansion and
344 activation of ILC3 during *Mtb* infection, our study reveals a more global alteration of
345 the ILC compartment in this context, including both ILC1 and ILC2. In particular, and
346 for the first time during *Mtb* infection, we report the plastic differentiation of ILC2, the
347 most prominent ILC subset in the mouse lung[2,35], toward ILC1-like cells. Differences
348 between the two studies may be due to the strains of *Mtb* used (HN878[34] *vs.* H37Rv
349 in our study), the markedly different proportions of the various ILC subsets in the lungs
350 reported in the two cases, or both.

351 Based on adoptive transfer experiments as well as on the ability of NMU to promote
352 ILC1-like cells, we found that ILC1-like cells appearing during *Mtb* infection originate
353 from an ILC2 population. While the plastic differentiation of lung ILC2 to ILC1-like cells

354 has previously been reported in the influenza virus infection model, whether they
355 originate form mature or immature ILC2 was not addressed [14]. We now demonstrate
356 that mature (IL-5 producing) ILC2 display a very limited potential to differentiate into
357 ILC1-like cells as evidenced using a fate-mapping approach. As described in recent
358 reports[4,17], lung ILC2 is a complex and heterogeneous population of cells with a broad
359 spectrum of maturity. Although the identity of the immature ILC2 population giving rise
360 to ILC1-like cells remains to be formally demonstrated, we identified an immature ILC2
361 subset, based on the expression of IL-18Rα, sharing phenotypic similarities with bone
362 marrow ILC2P, which retains the ability to differentiate into ILC1-like cells. These
363 results raise the exciting possibility that local precursors formed by immature ILC2 may
364 undergo an *ILCpoiesis*[16,17] controlled by the inflammatory context that may drive the
365 generation of ILC subsets adapted to *Mtb* infection in the lungs, as suggest in human
366 ILC biology[36,37]. In this regard, type 1 or type 2 environments triggered by cytokines
367 drove the conversion of IL-18Rα^+ ILC2 toward mature ILC2 or ILC1-like cells,
368 respectively. Although the potential of immature ILC2 to generate various ILC
369 populations was demonstrated *in vitro*, to our knowledge, our report is the first to show
370 the generation of ILC1-like cells from immature ILC2 *in vivo* in a relevant
371 pathophysiological setting.

372 The impact of infection-induced metabolic reprogramming on the phenotype of
373 immune cells represents a field of intense investigation, which remains particularly
374 focused on abundant cells, such as T lymphocytes and macrophages. In contrast, little
375 is known regarding how less abundant tissue-resident cells, such as ILCs, adapt to
376 their environment during infection to trigger an appropriate response[26]. Since *Mtb*
377 infection triggers major environmental changes[5,6], we questioned how metabolism
378 contributes to the plastic differentiation of ILC1-like cells.

379 We report for the first time that newly generated ILC1-like cells critically depend on
380 glycolytic metabolism that is independent of Arg1. Interestingly, glycolytic pathway is
381 also induced in ILC2, but in this case, it is rather associated with their inhibition. In this
382 case, Arg1, which is constitutively expressed by lung and bone marrow ILC2[27,38], was
383 linked to the ability of ILC2 to perform glycolysis and to sustain their functions[27].
384 However, the induction of HIF1α during ILC2 development in VHL-deficient mice
385 unfavored the acquisition of an ILC2 phenotype through metabolic and epigenetic

386 regulation[31]. Taken together, these results suggest that cells with a dramatically
387 different fate such as ILC2 and ILC1-like cells may rely on the same global metabolic
388 pathway. In fact, it seems that the association of metabolic machinery and metabolite
389 availability in tissues reflect the fate of ILC2 *vs.* ILC1-like cells. Indeed, we observed
390 that during type 1 inflammation, both ILC2 and ILC1-like cells express HIF1α but
391 stabilization of HIF1α in ILC2 favors an ILC1-like signature rather than stabilizing their
392 phenotype. Our results support the notion that HIF1α contributes to glycolysis
393 induction in both ILC2 and ILC1-like cells and in the generation and function of the
394 latter cell type. Glycolysis has been tightly connected to the production of IFN-γ by
395 various means such as epigenetic modification and post-transcriptional regulation of
396 *Ifng* mRNA[39,40]. In accordance, we report that DMOG-mediated stabilization of the
397 HIF1α protein in ILC2 *in vitro* favors both glycolysis induction and *Ifng* mRNA
398 expression. We found that *in vivo Ifng* mRNA was highly expressed in ILC1-like cells
399 and correlated with high *Hif1a* mRNA expression in these cells. While the HIF1α
400 protein expression could not be directly addressed *in vivo*, these results strongly
401 suggest that the HIF1α protein is stabilized in ILC1-like cells and is implicated in
402 glycolysis induction and, subsequently, IFN-γ production. Different levels of mtROS
403 found in IL-18Rα^- ILC2, IL-18Rα^+ ILC2, and ILC1-like cells corroborate this hypothesis.
404 Supporting this notion, *ex vivo* stimulation of ILC1-like cells in the presence of a
405 glycolysis inhibitor blocks IFN-γ production by these cells.

406 Collectively our results highlight the role played by environmental changes imposed
407 by inflammatory and/or metabolic programs on the fate and function of tissue-resident
408 ILCs. Future studies will aim at understanding the intrinsic and extrinsic molecular
409 mechanisms at play during this process. Our observation that BCG vaccination favors
410 the early generation of ILC1-like cells and that ILC1-like cell are endowed with a
411 protective potential during *Mtb* infection pave the way for future studies aiming at
412 elucidating the role played by ILC1-like cells in protection. On a broader perspective,
413 targeting ILC1-like cells using dedicated strategies may help develop novel
414 approaches to influence pathological situations where their emergence is favored.

415

416 **Materials & Methods**

417 **Mice**

418

419 Six-to-eight-week-old female C57BL/6 mice were purchased from Charles River
420 Laboratories France (Saint Germain Nuelles, France). *Rag2*$^{-/-}$ (B6.129-Rag2tm1Fwa),
421 *Rag2*$^{-/-}$*Il2rg*$^{-/-}$ (C;129S4-Rag2tm1.1Flv Il2rgtm1.1Flv/J), Red5 mice (B6(C)-
422 Il5tm1.1(icre)Lky/J)n, *Stat1*$^{-/-}$ (B6.129S(Cg)-Stat1tm1Dlv/J) and *Tbx21*$^{flox/flox}$ (B6.129-
423 Tbx21tm2Srnr/J) mice on a C57BL/6 J were bred in our animal facility. C3HeB/FeJ,
424 and ROSA26-YFP mice (B6.129X1-*Gt(ROSA)26Sor*$^{tm1(EYFP)Cos}$/J; 006148) were
425 purchased from The Jackson Laboratory through Charles Rivers Laboratory France.
426 All mice were maintained in specific-pathogen-free animal facility at IPBS and all
427 experiments were conducted in strict accordance with French laws and regulations in
428 compliance with the European Community council directive 68/609/EEC guidelines
429 and its implementation in France under procedures approved by the French Ministry
430 of Research and the FRBT (C2EA-01) animal care committee (APAFIS #1269, #3873,
431 #10546, #16529 and #17384).

432

433 ***Mtb* culture, immunization & mouse infections**

434

435 The laboratory strain of *Mtb*, H37Rv, was grown at 37°C in Middlebrook 7H9 medium
436 (Difco) supplemented with 10% albumin-dextrose-catalase (ADC, Difco) and 0.05%
437 Tyloxapol (Sigma), or on Middlebrook 7H11 agar medium (Difco) supplemented with
438 10% oleic acid-albumin-dextrose-catalase (OADC, Difco). Six- to eight-week-old mice
439 were anesthetized with a cocktail of ketamine (60 mg/kg, Merial) and xylasine (10
440 mg/kg, Bayer) and infected intranasally (i.n.) with 1000 CFUs of mycobacteria in 25 µL
441 of PBS containing 0.01% Tween 80. For immunization, C57BL/B6 mice were
442 immunized i.n. with 5.10^5 CFU of BCG (Danish), and were challenged 60 days post-
443 vaccination with H37Rv as previously described[33]. All experiments using *Mtb* were
444 performed in appropriate biosafety level 3 (BSL3) laboratory and animal facility.

445

446 ***In vivo* treatments**

447

448 Mice were injected intraperitoneally (i.p) one day before infection with either 100 µg of
449 mAb to NK1.1 (PK136, BioXcell) or 200 µg of mAb to IFNγ (BioXcell) or its isotype
450 control and the procedure was repeated twice a week until completion of the
451 experiment and sacrifice of the mice. 2-DG (1g/kg, Sigma) was injected every other
452 day starting from the day of infection and until completion of the experiment. For
453 glucose supplementation, mice were treated with drinking water containing 30% (w/v)
454 glucose (started 1 week before infection until sacrifice).
455
456 **Adoptive transfer experiments**
457
458 For the adoptive transfer of ILCs, *in vitro* cultured ILC2 were harvested after 7 days of
459 culture and $5x10^5$ to $2x10^6$ cells were transferred i.v. in mice anesthetized with
460 isoflurane one day before *Mtb* infection in *Rag2*$^{-/-}$*Il2rg*$^{-/-}$. For ILC1-like transfer, $1x10^4$
461 purified ILC1-like were directly transferred via intratracheal (i.t.) route in mice
462 anesthetized with isoflurane one day before *Mtb* infection in *Rag2*$^{-/-}$*Il2rg*$^{-/-}$.
463
464 **Lung harvest**
465
466 Mice were sacrificed any cervical dislocation under isoflurane anesthesia and lungs
467 were harvested aseptically, homogenized using a gentleMACS dissociator (C Tubes,
468 Miltenyi) in HBSS (Difco), and incubated with DNAse I (0.1 mg/mL, Roche) and
469 collagenase D (2 mg/mL, Roche) during 30 min at 37°C under 5% CO2. When
470 indicated, mice received an i.v. injection of labeled anti-CD45 mAb (5µg) 5 minutes
471 before sacrifice to discriminate between parenchymal and intravascular cells in
472 subsequent flow cytometry analyses. Lungs homogenates were filtered on 40 µm cell
473 strainers and centrifuged at 329 × g during 5 min. Supernatants were conserved for
474 cytokine content analysis. A part of the cellular pellet was conserved in TRIzol reagent
475 for cellular RNA analysis. Bacterial loads (colony forming units) were determined by
476 plating serial dilutions of the lung homogenates onto 7H10 solid medium (Difco)
477 supplemented with 10% oleic acid-albumin-dextrose-catalase (OADC, Difco). The
478 plates were incubated at 37°C for 3 weeks before bacterial CFUs scoring. In the
479 remaining fraction, red blood cells were lysed in 150 mM NH4Cl, 10 mM $KHCO_3$, 0.1
480 mM EDTA (pH 7.2) for immunological staining.
481

482 ***In situ* expansion of ILC**

483

484 To expand ILC2, C57BL/6 or *Rag2*$^{-/-}$ mice were treated intranasally (i.n.) with 100 ng
485 of recombinant IL-33 (Biolegend) each day for 5 consecutive days. For the cytokine-
486 based plasticity model, C57BL/6 or *Rag2*$^{-/-}$ mice were treated i.n. with different
487 combinations of cytokines specified in figures legends at day 1, 3, 5, 8 and sacrificed
488 at day 9: 100 ng of IL-12 (R&D), IL-18 (R&D), IL-33 (Biolegend), IFNγ (Biolegend) or
489 20 µg of NMU (US Biological) per mouse and per instillation. For the Seahorse assays
490 we elicited ILC2 with 0.5 mg IL-33, three doses i.p. over 10 days. Sorted ILC2 from
491 lung were then cultured in presence of IL-7 and IL-2 (50ng/ml) for 7 days before
492 addition of DMOG.

493

494

495 **Flow cytometry**

496

497 To identify mouse ILCs, single-cell suspensions were stained with mAb for known
498 lineages and with mAb discriminating ILC subsets. mAbs for known lineages included
499 CD3 (17A2, Biolegend), CD4 (RM4-5, Biolegend), CD8a (53-6.7, Biolegend), TCRαβ
500 (H57-597, Biolegend), TCRγδ, (GL3, Biolegend) CD11b (M1/70, Biolegend), CD11c
501 (N418, Biolegend), F4/80 (BM8, Biolegend), Ly6G (1A8, Biolegend), TER119 (TER-
502 119, Biolegend), FcεRIa (MAR-1, Biolegend), CD19 (1D3/CD19, Biolegend), B220
503 (RA3-6B2, Biolegend), and CD49b (DX5, Biolegend). mAbs discriminating ILC subsets
504 included CD45.2 (104, BD), CD90.2 (30-H12, Biolegend), CD127 (A7R34,
505 eBioscience), NK1.1 (PK136, BD Biosciences), IL-18Rα (P3TUNYA, eBioscience),
506 ST2 (RMST2-2, eBioscience), CD226 (10E5, Biolegend), CD49a (Ha31/8), NKp46
507 (29A1.4), KLRG1 (2F1, eBiosciences), and ICOS (C398.4A, Biolegend).
508 mAbs for intracellular staining included GATA3 (L50-823, BD Biosciences), T-bet
509 (4B10, eBiosciences), RORγt (Q31-378, BD Biosciences), PLZF (9E12, Biolegend),
510 TCF-1 (S33-966, BD), Arg1 (A1exF5, BD Biosciences), Ki-67 (SolA15, eBiosciences),
511 Eomes (Dan11mag, eBiosciences, and HIF1α (D1S7W, Cell Signaling). After
512 extracellular staining, cells were fixed and permeabilized (Foxp3 staining kit,
513 eBiosciences) for intracellular staining. Samples from Biosafety Level 3 were
514 inactivated for 2 hours at RT with 4% paraformaldehyde (ThermoFisher Scientific) after
515 extracellular and intracellular staining.

516 Live/Dead fixable blue (eBiosciences) and mouse FcBlock (BD Biosciences) were
517 used for all flow cytometry experiments. Cell staining was analyzed using LSR
518 Fortessa flow cytometers (BD) and FlowJo software (v10). Cells were first gated in
519 singlets (FSC-H vs. FSC-W and SSC-H vs. SSC-W) and live cells before further
520 analyses.
521
522 **Intracellular cytokines staining**
523
524 For intracellular cytokines staining of ILCs, single-cell suspensions from lung were
525 incubated at 37°C with Brefeldin A in association or not with PMA (50 ng/ml,
526 Sigma)/Ionomycine (500 ng/ml, Sigma) or 50 ng/ml of IL-12 and IL-18 for 4 hours
527 before being surface stained, fixed and permeabilized (Foxp3 staining kit,
528 eBiosciences). mAbs for cytokines staining included IFN-γ (XMG1.2, Biolegend), IL-
529 17A (TC11-18H10, BD Biosciences), IL-5 (TRFK5, BD Biosciences), and IL-13
530 (eBio13A, eBiosciences) To block glycolysis during *ex vivo* stimulation, cells were
531 incubated in the presence of 10mM 2-DG (Sigma). *Mtb was* inactivated by incubation
532 in PFA 4% for 2 hours at room temperature. For analyses of mitochondrial markers,
533 cells were stained with MitoSOX Red (5 µM, eBiosciences) at 37°C for 30min.
534
535 **Detection of mRNA using PrimeFlow**
536
537 For PrimeFlow (ThermoFisher Scientific) experiments, single cell suspensions of lungs
538 were analyzed for mRNA expression after extracellular/intracellular staining using the
539 PrimeFlow RNA assay (eBioscience) and standard mouse probe sets for *Ifng*, *Il5,* and
540 *Hif1a,* according to manufacturer's instructions for 96-well-plate staining.
541
542 **ILC enrichment and cell-sorting**
543
544 Lung ILCs were enriched from lung single-cell suspensions by using the EasySep™
545 Mouse ILC2 Enrichment Kit (StemCell). After enrichment, cells were stained with
546 lineage mAb (CD3, CD4, CD8a, TCRαβ, TCRγδ, CD19, B220, CD11b, CD11c, F4/80,
547 TER119, FcεRIa, CD49b, Ly6G) and ILC markers (CD90.2, CD45.2, NK1.1, ST2, IL-
548 18Rα, CD49a). ILC2 were purified as $Lin^{-}CD45.2^{+}CD90.2^{+}NK1.1^{-}ST2^{+}$. ILC1-like were

549 purified as Lin$^-$CD45.2$^+$CD90.2$^+$NK1.1$^-$ST2$^+$CD49a$^+$IL-18Rα$^+$. Cells were sorted using a
550 FACSAria Fusion cytometer (BD, France).
551
552 ***In vitro* culture of ILC2**
553
554 Cell sorted ILC2 were incubated in 6-well plates at a density of 300,000 cells per ml
555 for 4 days with IL-2 (25 ng/ml, R&D) and IL-7 (25 ng/ml, R&D) in RPMI (Difco)
556 supplemented with 10 % FBS. After 4 days of culture, ILC2 were harvested for adoptive
557 transfer or incubated with DMOG (Sigma). For DMOG experiment, half of the medium
558 was removed and replaced with fresh medium containing IL-2 (25 ng/ml) and IL-7 (25
559 ng/ml) with or without DMOG (500 µg/ml) for 3 more days. Cell sorted ILC2 were
560 incubated in 6-well plates at a density of 300,000 cells per ml for 4 days with IL-2 (25
561 ng/ml, R&D) and IL-7 (25 ng/ml, R&D) in RPMI (Difco) supplemented with 10 % FBS.
562 After 4 days of culture, ILC2 were harvested for adoptive transfer or incubated with
563 DMOG (Sigma). For DMOG experiment, half of the medium was removed and
564 replaced with fresh medium containing IL-2 (25 ng/ml) and IL-7 (25 ng/ml) with or
565 without DMOG (500 µg/ml) for 3 more days. For the Seahorse assays, sorted ILC2
566 from lung were cultured in presence of IL-7 and IL-2 (50ng/ml) for 7 days before
567 addition of DMOG.
568
569
570 **SCENITH assay**
571
572 SCENITH experiments were performed as previously described[28] using the SCENITH
573 kit containing all reagents and anti-puromycin antibodies (requested from
574 www.scenith.com/try-it). Briefly, lung cell suspensions were stimulated for 15 minutes
575 at 37°C in the presence of the indicated inhibitors of various metabolic pathways then
576 incubated for 30 minutes with puromycin at 37°C. At the end of the incubation,
577 puromycin was stained with fluorescent anti-puromycin antibodies (Clone R4743L-E8)
578 by flow cytometry and the impact of the various metabolic inhibitors was quantitated
579 as described[28].
580
581 **Seahorse experiments**
582

583 1.5 to 2 x10^5 FACS sorted lung ILC2s per well were rested in a 96-well plate in
584 Glutamax RPMI (supplemented with 10% fetal bovine serum, non-essential amino
585 acids, 1 mM sodium pyruvate, 85 µM 2-mercapto-ethanol and 100 U/ml penicillin-
586 streptomycin) containing 25 ng/ml IL-7. After 24h cells were split and rested in fresh
587 IL-7 containing media for another 3 days. Subsequently, cells were cultured in fresh
588 medium containing 25 ng/ml IL-7 and 20 ng/ml of IL-2 in the presence or absence of
589 0.5 mM DMOG for a further 72 hours. To prepare for extracellular flux analysis cells
590 were then washed thoroughly in XF medium (modified DMEM) and adhered to the
591 Seahorse plate using 22.4 µg/ml Cell-Tak (Corning).

592 For glycolytic stress test, cells were plated at a density of 2x10^5 cells/well in XF medium
593 supplemented with 2 mM glutamine. Cells were incubated for 30-60 min at 37°C and
594 ECAR was measured under basal conditions, and in response to 10 mM glucose, 2
595 µM oligomycin and 50 mM 2-DG. For the mitochondrial stress test, cells were plated
596 at a density of 1.5x10^5 cells/well in XF medium supplemented with 2 mM glutamine, 1
597 mM sodium pyruvate and 25 mM glucose. Cells were incubated for 30-60 min at 37°C.
598 OCAR was measured under basal conditions, after injection of 2 µM oligomycin, 1.5
599 µM FCCP and 100 nM rotenone + 1 µM antimycin A. Extracellular flux assays were
600 done using a 96-well extracellular flux analyzer XFe-96 (Seahorse Bioscience).

601 Normalization by protein was used to correct for potential differences in seeding
602 densities across wells. Protein measurement was performed using the Pierce BCA
603 protein assay according to the manufacturer instructions.

604 **Quantification of cytokine production by ELISA**

605

606 Secreted cytokines from *Mtb*-infected lung supernatant were measured by ELISA
607 assays using kits from BD Bioscience (IFN-γ), according to the manufacturer's
608 instructions.

609

610 ***In vitro* differentiation of ILC2P**

611

612 To induce the ILC2 differentiation *in vitro*, bone marrow cells (BM) were collected from
613 hips, femurs and tibias. ILC2P were FACS-sorted from magnetically-enriched Sca^+
614 cells (Lin^-, $Sca1^+$ ckit dull, $CD127^+$, $CD25^+$). Purified ILC2P were cultured for 7 days in

615 aMEM complete medium (10% heat-inactivated FCS, 1% penicillin-streptomycin, 50
616 μM β-mercaptoethanol) on OP9-DL1, with 10 ng/ml of IL-7 and 10 ng/ml of SCF. In
617 addition, depending on the experimental condition mouse IL-33 (10 ng/ml), mouse IL-
618 12 (10 ng/ml), mouse IL-18 (10 ng/ml), mouse IFN-γ (10 ng/ml) have been added.

619 **Quantitative RT-PCR analysis of transcripts**

620

621 RNA from lungs homogenates was extracted using TRIzol reagent (Ambion) and
622 RNeasy spin columns according to manufacturer's instructions (RNeasy kit, Qiagen).
623 RNA was reverse transcribed into cDNA using M-MLV Reverse transcriptase
624 (Invitrogen). RT-qPCR was performed using gene-targeted primers (Supplementary
625 Table 1) as described above. Values were normalized using the housekeeping beta-
626 actin gene (*Actb*) and expressed as a fold change. RNA from ILC2 culture were
627 extracted using RLT (Qiagen) and RNA were reverse transcribed as previously
628 described [41].

629

630 **Statistical analyses**

631

632 Statistical analyses were performed using GraphPad Prism 9 software. Agostino and
633 Pearson normality tests were performed to determine whether data followed a normal
634 distribution. Unpaired *t*-test (for normal data) or Mann-Whitney (for non-normal data)
635 were performed when two samples were compared; ANOVA (for normal data) or
636 Kruskal-Wallis (for non-normal data) tests were performed when more than two
637 samples were compared. For all analyses, * indicates $P < 0.05$, ** indicates $P < 0.01$,
638 *** indicates $P < 0.001$, and **** indicates $P < 0.0001$.

639

640 **Acknowledgements**

641

642 We acknowledge Emmanuelle Näser (TRI-IPBS platform, Toulouse) for flow
643 cytometry and imagery analyses, Flavie Moreau, Céline Berrone and Aline Tridon
644 (Anexplo-IPBS platform, Toulouse), and Sylvie Appolinaire and Celine Berraud
645 (CREFRE animal facility, Toulouse) for mouse care and maintenance in conventional
646 and BSL3 facilities. We thank Anne Dejean (CPTP, INSERM, Toulouse) for the kind
647 gift of *Tbx21*$^{fl/fl}$ mice, Etienne Meunier (IPBS, CNRS, Toulouse) for the kind gift of *Stat1*$^{-}$

648 /- mice and Richard Locksley (USCF, San Francisco) for the kind gift of Red5 mice. We
649 thank Juan Carlos Zúñiga-Pflücker, University of Toronto for the kind gift of OP9-DL1
650 cells. We thank Geanncarlo Lugo-Villarino, Pauline Schmitt (IPBS, Toulouse), Sophie
651 Laffont (CPTP, Toulouse) and Andrea Pichler (CRCT, Toulouse) for helpful discussion.
652 This work was supported by Centre de la Recherche Scientifique (CNRS), the
653 University of Toulouse, University Toulouse-III, Paul Sabatier, the French Ministry of
654 Higher Education, Research and Innovation (Fellowship to D.C.), the Fondation pour
655 la Recherche Médicale (DEQ20160334902 to ON), the Bettencourt Schueller
656 Foundation (Grants Coup d'Élan pour la recherche française and Explore-TB to ON),
657 MSDAVENIR (Grant Fight-TB to ON), the Agence Nationale de la Recherche (ANR-
658 18-CE15-0004-01 to DH and ANR-11-EQUIPEX-0003 to ON), and the European
659 Commission (TBVAC2020 n°643381 to ON). MRH is supported by a Royal Society
660 and Wellcome Trust Sir Henry Dale Fellowship (105644/Z/14/Z), a Lister Institute of
661 Preventative Medicine Prize and a BBSRC Project Grant (BB/T014482/1). The funders
662 had no role in study design, data collection, and analysis, decision to publish, or
663 preparation of the manuscript. This manuscript was edited at Life Science Editors.
664

665 **Author contributions**

666

667 D.C. and D.H. conceived and designed the study with input from O.N. ; D.C., A.C.,
668 M.Z.K., E.B., and F.L. performed the experiments ; E.L., J-P.G., and R.J.A contributed
669 critical reagents and methods, D.C., G.E., J-C.G., R.J.A., M.R.H. and D.H. analyzed
670 and interpreted the data; J-C.G., G.E., M.R.H., and Y.P., also provide important
671 discussion for the project and critical feedback on the manuscript ; D.C., O.N. and D.H.
672 wrote the manuscript. All coauthors read, reviewed and approved the manuscript.
673

674 **Competing interests**

675

676 The authors declare no competing interests
677

678 **References**

679 1. Meininger, I. *et al.* Tissue-Specific Features of Innate Lymphoid Cells. *Trends*
680 *Immunol.* **41**, 902–917 (2020).
681 2. Vivier, E. *et al.* Innate Lymphoid Cells: 10 Years On. *Cell* **174**, 1054–1066
682 (2018).
683 3. Shih, H.-Y. *et al.* Developmental Acquisition of Regulomes Underlies Innate
684 Lymphoid Cell Functionality. *Cell* **165**, 1120–1133 (2016).
685 4. Ricardo-Gonzalez, R. R. *et al.* Tissue signals imprint ILC2 identity with
686 anticipatory function. *Nat. Immunol.* **19**, 1093–1099 (2018).
687 5. Shi, L. *et al.* Infection with Mycobacterium tuberculosis induces the Warburg
688 effect in mouse lungs. *Sci. Rep.* **5**, 1–13 (2015).
689 6. Fernández-García, M. *et al.* Comprehensive Examination of the Mouse Lung
690 Metabolome Following Mycobacterium tuberculosis Infection Using a Multiplatform
691 Mass Spectrometry Approach. *J. Proteome Res.* **19**, 2053–2070 (2020).
692 7. Svedberg, F. R. *et al.* The lung environment controls alveolar macrophage
693 metabolism and responsiveness in type 2 inflammation. *Nat. Immunol.* **20**, 571–580
694 (2019).
695 8. Saluzzo, S. *et al.* First-Breath-Induced Type 2 Pathways Shape the Lung
696 Immune Environment. *Cell Rep.* **18**, 1893–1905 (2017).
697 9. O'Garra, A. *et al.* The Immune Response in Tuberculosis. *Annu. Rev. Immunol.*
698 **31**, 475–527 (2013).
699 10. Orme, I. M., Roberts, A. D., Griffin, J. P. & Abrams, J. S. Cytokine secretion by
700 CD4 T lymphocytes acquired in response to Mycobacterium tuberculosis infection. *J.*
701 *Immunol.* **151**, 518–525 (1993).
702 11. Martínez-Barricarte, R. *et al.* Human IFN-γ immunity to mycobacteria is
703 governed by both IL-12 and IL-23. *Sci. Immunol.* **3**, (2018).
704 12. Urdahl, K., Shafiani, S. & Ernst, J. Initiation and regulation of T-cell responses
705 in tuberculosis. *Mucosal Immunol.* **4**, 288–293 (2011).
706 13. Bal, S. M., Golebski, K. & Spits, H. Plasticity of innate lymphoid cell subsets.
707 *Nat. Rev. Immunol.* 1–14 (2020) doi:10.1038/s41577-020-0282-9.
708 14. Silver, J. S. *et al.* Inflammatory triggers associated with exacerbations of COPD
709 orchestrate plasticity of group 2 innate lymphoid cells in the lungs. *Nat. Immunol.* **17**,
710 626–635 (2016).

711 15. Nussbaum, J. C. *et al.* Type 2 innate lymphoid cells control eosinophil
712 homeostasis. *Nature* **502**, 245–248 (2013).
713 16. Ghaedi, M. *et al.* Single-cell analysis of RORα tracer mouse lung reveals ILC
714 progenitors and effector ILC2 subsets. *J. Exp. Med.* **217**, (2020).
715 17. Zeis, P. *et al.* In Situ Maturation and Tissue Adaptation of Type 2 Innate
716 Lymphoid Cell Progenitors. *Immunity* **53**, 775-792.e9 (2020).
717 18. Weizman, O.-E. *et al.* ILC1 Confer Early Host Protection at Initial Sites of Viral
718 Infection. *Cell* **171**, 795-808.e12 (2017).
719 19. Chiossone, L., Dumas, P.-Y., Vienne, M. & Vivier, E. Natural killer cells and
720 other innate lymphoid cells in cancer. *Nat. Rev. Immunol.* **18**, 671–688 (2018).
721 20. Kinjo, Y. *et al.* Contribution of IL-18 to Th1 response and host defense against
722 infection by Mycobacterium tuberculosis: a comparative study with IL-12p40. *J.*
723 *Immunol. Baltim. Md 1950* **169**, 323–329 (2002).
724 21. Duerr, C. U. *et al.* Type I interferon restricts type 2 immunopathology through
725 the regulation of group 2 innate lymphoid cells. *Nat. Immunol.* **17**, 65–75 (2016).
726 22. Moro, K. *et al.* Interferon and IL-27 antagonize the function of group 2 innate
727 lymphoid cells and type 2 innate immune responses. *Nat. Immunol.* **17**, 76–86 (2016).
728 23. Cardoso, V. *et al.* Neuronal regulation of type 2 innate lymphoid cells via
729 neuromedin U. *Nature* **549**, 277–281 (2017).
730 24. Klose, C. S. N. *et al.* Differentiation of Type 1 ILCs from a Common Progenitor
731 to All Helper-like Innate Lymphoid Cell Lineages. *Cell* **157**, 340–356 (2014).
732 25. Wallrapp, A. *et al.* The neuropeptide NMU amplifies ILC2-driven allergic lung
733 inflammation. *Nature* **549**, 351–356 (2017).
734 26. Joseph, A. M., Monticelli, L. A. & Sonnenberg, G. F. Metabolic regulation of
735 innate and adaptive lymphocyte effector responses. *Immunol. Rev.* **286**, 137–147
736 (2018).
737 27. Monticelli, L. A. *et al.* Arginase 1 is an innate lymphoid-cell-intrinsic metabolic
738 checkpoint controlling type 2 inflammation. *Nat. Immunol.* **17**, 656–665 (2016).
739 28. Argüello, R. J. *et al.* SCENITH: A Flow Cytometry-Based Method to Functionally
740 Profile Energy Metabolism with Single-Cell Resolution. *Cell Metab.* **32**, 1063-1075.e7
741 (2020).
742 29. Heiden, M. G. V., Cantley, L. C. & Thompson, C. B. Understanding the Warburg
743 Effect: The Metabolic Requirements of Cell Proliferation. *Science* **324**, 1029–1033
744 (2009).

745 30. Palazon, A., Goldrath, A. W., Nizet, V. & Johnson, R. S. HIF Transcription
746 Factors, Inflammation, and Immunity. *Immunity* **41**, 518–528 (2014).
747 31. Li, Q. *et al.* E3 Ligase VHL Promotes Group 2 Innate Lymphoid Cell Maturation
748 and Function via Glycolysis Inhibition and Induction of Interleukin-33 Receptor.
749 *Immunity* **48**, 258-270.e5 (2018).
750 32. Muri, J. & Kopf, M. Redox regulation of immunometabolism. *Nat. Rev. Immunol.*
751 1–19 (2020) doi:10.1038/s41577-020-00478-8.
752 33. Perdomo, C. *et al.* Mucosal BCG Vaccination Induces Protective Lung-Resident
753 Memory T Cell Populations against Tuberculosis. *mBio* **7**, (2016).
754 34. Ardain, A. *et al.* Group 3 innate lymphoid cells mediate early protective immunity
755 against tuberculosis. *Nature* **570**, 528–532 (2019).
756 35. Stehle, C., Hernández, D. C. & Romagnani, C. Innate lymphoid cells in lung
757 infection and immunity. *Immunol. Rev.* **286**, 102–119 (2018).
758 36. Lim, A. I. *et al.* Systemic Human ILC Precursors Provide a Substrate for Tissue
759 ILC Differentiation. *Cell* **168**, 1086-1100.e10 (2017).
760 37. Lim, A. I. & Di Santo, J. P. ILC-poiesis: Ensuring tissue ILC differentiation at the
761 right place and time. *Eur. J. Immunol.* **49**, 11–18 (2019).
762 38. Bando, J. K., Nussbaum, J. C., Liang, H.-E. & Locksley, R. M. Type 2 innate
763 lymphoid cells constitutively express arginase-I in the naïve and inflamed lung. *J.*
764 *Leukoc. Biol.* **94**, 877–884 (2013).
765 39. Peng, M. *et al.* Aerobic glycolysis promotes T helper 1 cell differentiation through
766 an epigenetic mechanism. *Science* **354**, 481–484 (2016).
767 40. Chang, C.-H. *et al.* Posttranscriptional Control of T Cell Effector Function by
768 Aerobic Glycolysis. *Cell* **153**, 1239–1251 (2013).
769 41. Troegeler, A. *et al.* C-type lectin receptor DCIR modulates immunity to
770 tuberculosis by sustaining type I interferon signaling in dendritic cells. *Proc. Natl. Acad.*
771 *Sci. U. S. A.* **114**, E540–E549 (2017).
772

Figure 1

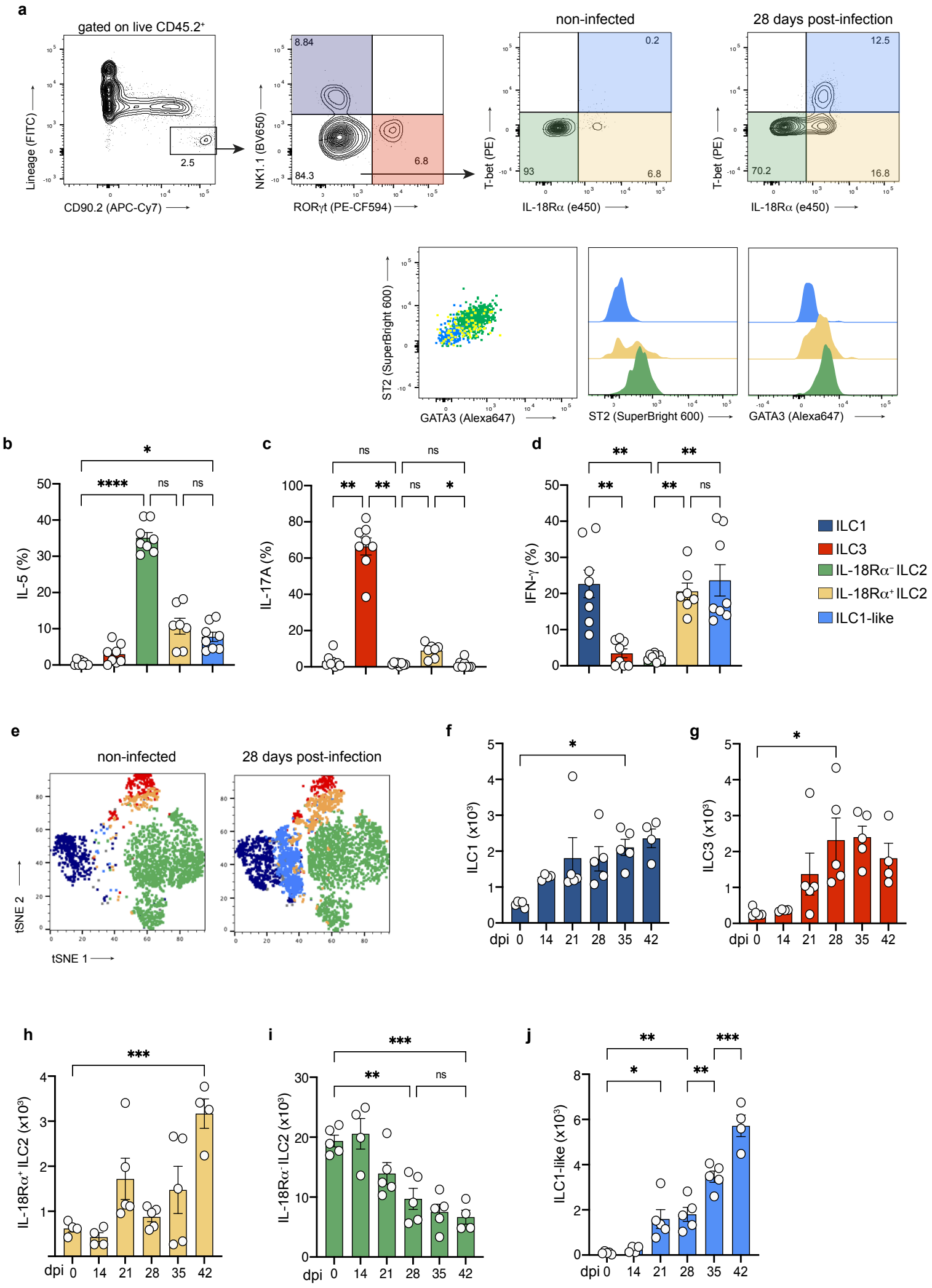
a
gated on live CD45.2+
Lineage (FITC)
CD90.2 (APC-Cy7)
2.5
NK1.1 (BV650)
RORγt (PE-CF594)
8.84
84.3
6.8
non-infected
28 days post-infection
T-bet (PE)
IL-18Rα (e450)
0.2
93
6.8
12.5
70.2
16.8
ST2 (SuperBright 600)
GATA3 (Alexa647)
b
IL-5 (%)
c
IL-17A (%)
d
IFN-γ (%)
ILC1
ILC3
IL-18Rα- ILC2
IL-18Rα+ ILC2
ILC1-like
e
non-infected
28 days post-infection
tSNE 1
tSNE 2
f
ILC1 (x10³)
g
ILC3 (x10³)
dpi 0 14 21 28 35 42
h
IL-18Rα+ ILC2 (x10³)
i
IL-18Rα- ILC2 (x10³)
j
ILC1-like (x10³)

Figure 1. IFN-γ**-producing ILC1-like cells emerge during *Mtb* infection. (a)** Representative dot plots showing the gating strategy used to analyze ILC subsets in the lungs of C57BL/6 mice after doublets exclusion (top graphs): ILC1 (dark blue), ILC3 (red), IL-18Rα$^-$ ILC2 (green), IL-18Rα$^+$ ILC2 (yellow) and T-bet$^+$IL-18Rα$^+$ ILC (light blue) are depicted in non-infected and *Mtb*-infected mice. Representative expression of GATA3 and ST2 on the indicated ILC subsets following the above color code) (bottom graphs). **(b-d)** Percentage of IL-5 (b), IL-17A (c), and IFN-γ (d) in the indicated ILC subsets at day 28 post-infection in C57BL/6 mice. **(e)** Unsupervised t-SNE distribution of total lung Lin$^-$CD90.2$^+$ populations at steady-state (left graph) and during *Mtb* infection (right graph). Based on gating strategy defined in Fig.1a, ILC subsets were depicted with the same color code: ILC1 in dark blue, ILC3 in red, IL-18Rα$^-$ ILC2 in green, IL-18Rα$^+$ ILC2 in yellow and ILC1-like cells (light blue). **(f-j)** Absolute numbers of ILC1 (f), ILC3 (g), IL-18Rα$^+$ ILC2 (h), IL-18Rα$^-$ ILC2 (i), and ILC1-like cells (j) at the indicated days after *Mtb* infection. Prior to sacrifice, mice were injected with fluorescent anti-CD45.2 to distinguish vascular and parenchymal cells. ILC1, ILC3, IL-18Rα$^-$ ILC2 and IL-18Rα$^+$ ILC2 have been gated on lung-resident cells. In **(b-d, f-j)**, data are representative of five independent experiments with each symbol representing an individual mouse, graphs depict data as mean (± s.e.m) and statistical analysis was performed using two-way ANOVA (*, $p<0.05$; **, $P<0.01$; ***, $p<0.001$; ****, $p<0.0001$).

Figure 2

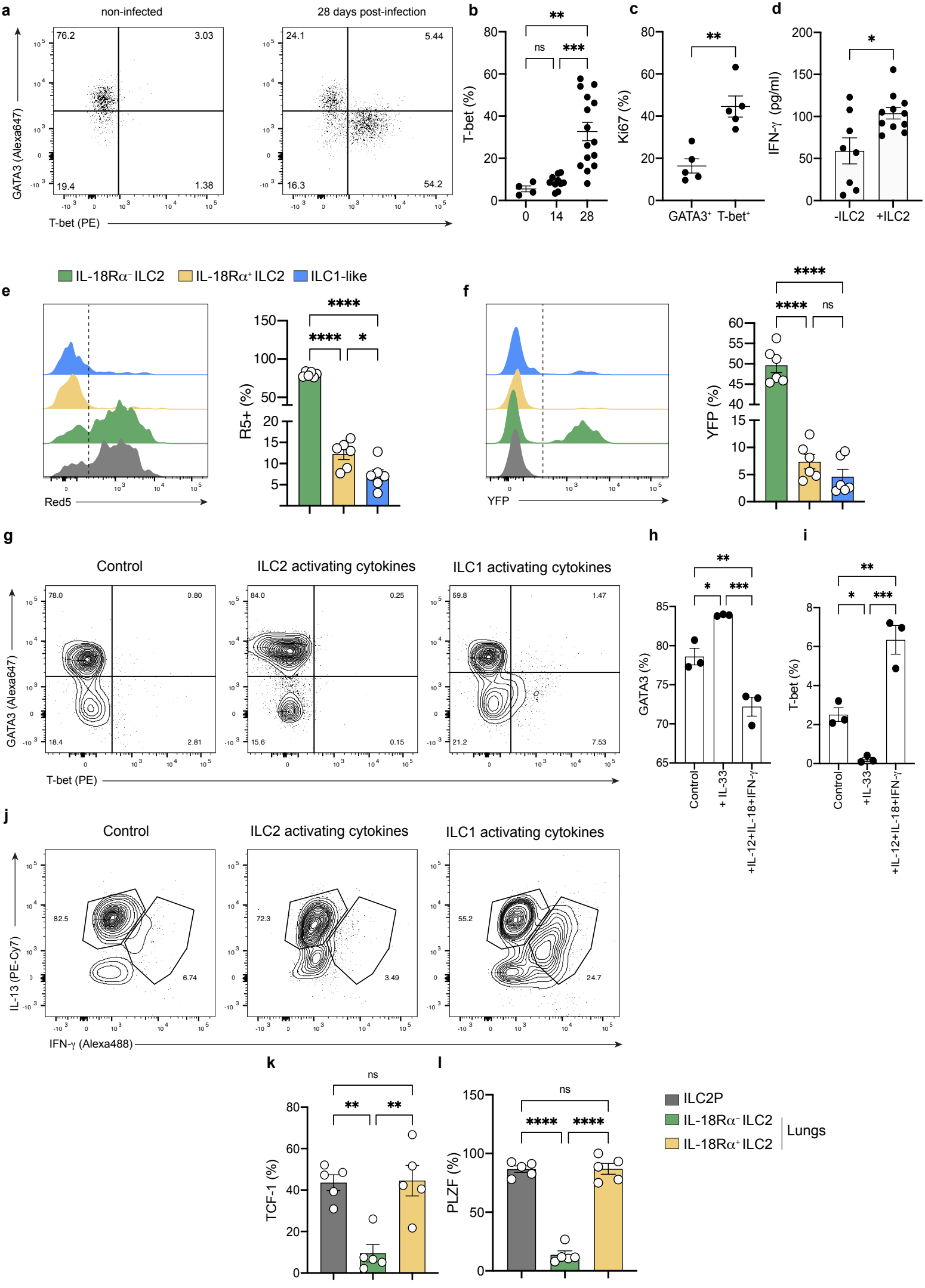
a
non-infected
28 days post-infection
GATA3 (Alexa647)
T-bet (PE)
76.2
3.03
19.4
1.38
24.1
5.44
16.3
54.2
b
T-bet (%)
ns
**
***
0
14
28
c
Ki67 (%)
**
GATA3+
T-bet+
d
IFN-γ (pg/ml)
*
-ILC2
+ILC2
IL-18Rα- ILC2
IL-18Rα+ ILC2
ILC1-like
e
Red5
R5+ (%)
****
*
f
YFP
YFP (%)
ns
g
Control
ILC2 activating cytokines
ILC1 activating cytokines
78.0
0.80
18.4
2.81
84.0
0.25
15.6
0.15
69.8
1.47
21.2
7.53
h
GATA3 (%)
Control
+ IL-33
+IL-12+IL-18+IFN-γ
i
T-bet (%)
j
IL-13 (PE-Cy7)
IFN-γ (Alexa488)
82.5
6.74
72.3
3.49
55.2
24.7
k
TCF-1 (%)
l
PLZF (%)
ILC2P
IL-18Rα- ILC2
IL-18Rα+ ILC2
Lungs

Figure 2. ILC2 give rise to ILC1-like cells during *Mtb* infection. (a) A representative dot-plot of GATA3 and T-bet expression in Lin$^-$CD45.2$^-$CD90.2$^-$ cells isolated from *Rag2*$^{-/-}$*Il2rg*$^{-/-}$ mice adoptively transferred with purified ILC2 then left uninfected (right) or infected with *Mtb* (left). **(b)** Percentages of T-bet expressing ILC at different days post-infection. **(c)** Percentages of Ki67$^+$ cells among GATA3^{hi}T-bet^{low} and GATA3^{low}T-bet^{hi} cells. **(d)** Concentration of IFN-γ determined by ELISA in total lungs from *Mtb*-infected *Rag2*$^{-/-}$*Il2rg*$^{-/-}$ mice transferred (+ILC2) or not (-ILC2) with purified ILC2, the ELISA results were pooled from two independent experiments. **(e-f)** Representative histograms showing IL-5 (e) and YFP (f) expression among IL-18Rα^- ILC2 (green), IL-18Rα^+ ILC2 (yellow), and ILC1-like (blue) in non-infected *vs*. *Mtb*-infected IL-5^{Cre}ROSA26^{YFP} mice. Grey histograms represent IL-5 (e) or YFP (f) expression in IL-18Rα^- ILC2 in IL-5^{Cre} mice. Vertical dotted line indicates the threshold determining positivity. Bar graphs show percentages of IL-5 (e) or YFP (f) cells in IL-18Rα^- ILC2 (green), IL-18Rα^+ ILC2 (yellow), and ILC1-like (blue) at day 28 post-infection in IL-5^{Cre}ROSA26^{YFP}. **(g)** Representative dot-plot showing GATA3 and T-bet expression in bone marrow ILCP in an *in vitro* differentiation assay performed in control conditions or in the presence of ILC2 or ILC1 activating cyokines. **(h-i)** Expression of GATA3 **(h)** and T-bet **(i)** in bone marrow ILC2P after 7 days of culture with IL-7/SCF ± IL-33 ± IL-12/IL-18/IFN-γ . **(j)** Representative dot-plot showing IL-13 and IFN-γ expression in bone marrow ILC2P in an *in vitro* differentiation assay under the indicated conditions after *ex vivo* stimulation with PMA/ionomycin. (k-l) Percentage of TCF-1 **(k)** and PLZF **(l)** in ILC2P from bone marrow (grey) compared to IL-18Rα^- ILC2 (green) and IL-18Rα^+ ILC2 (yellow) from lungs of C57BL/6 mice at steady-state. Each symbol represents an individual mouse **(b, c, d, e, f, k, l)** or biological replicates (**h, i**). Statistical analysis was performed using Anova two-way **(b, e, f, h, i, k, l)** and Mann-Whitney test **(c, d)** (*, $p<0.05$; **, $P<0.01$; ***, $p<0.001$; ****, $p<0.0001$). Graphs depict data as mean (± s.e.m). Data are representative of three **(b, c)**, two **(g-l),** a pool of two **(d)** independent experiments and one experiment with 6 mice per group (e ,f).

Figure 3

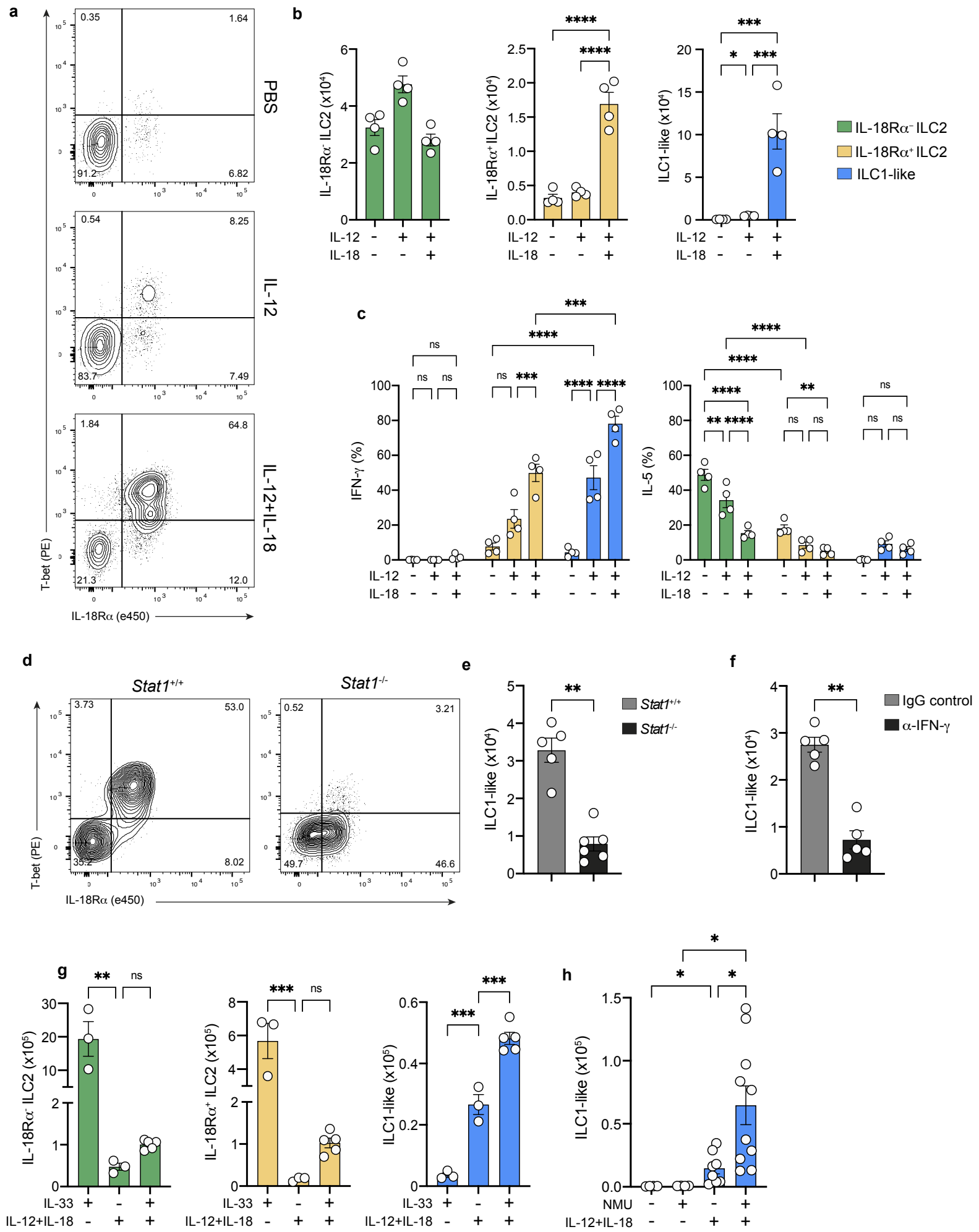
a
PBS
IL-12
IL-12+IL-18
T-bet (PE)
IL-18Rα (e450)
b
IL-18Rα⁻ ILC2 (x10⁴)
IL-18Rα⁺ ILC2 (x10⁴)
ILC1-like (x10⁴)
IL-12
IL-18
IL-18Rα⁻ ILC2
IL-18Rα⁺ ILC2
ILC1-like
c
IFN-γ (%)
IL-5 (%)
d
Stat1+/+
Stat1-/-
e
ILC1-like (x10⁴)
f
IgG control
α-IFN-γ
g
IL-18Rα⁻ ILC2 (x10⁵)
IL-18Rα⁺ ILC2 (x10⁵)
ILC1-like (x10⁵)
IL-33
IL-12+IL-18
h
NMU

Figure 3. The inflammatory environment shapes the fate of immature ILC2. (a) Representative dot-plots of T-bet and IL18Rα expression after intranasal administration of PBS, IL-12, and IL-12+IL-18 in *Rag2*$^{-/-}$ mice. **(b)** Absolute numbers of IL-18Rα^{-} ILC2 (green), IL-18Rα^{+} ILC2 (yellow) and ILC1-like cells (blue) after cytokine treatment or control (PBS). **(c)** Percentages of cells expressing IFN-γ (left) or IL-5 (right) among the indicated ILC subsets after *ex vivo* stimulation with PMA/ionomycin in the presence of brefeldin A for 4h. **(d)** Representative dot-plot of T-bet and IL-18Rα expression in *Stat1*$^{+/+}$ *vs. Stat1*$^{-/-}$ mice after intranasal administration of IL-12 and IL-18. **(e)** Absolute numbers of ILC1-like cells in *Stat1*$^{+/+}$ *vs. Stat1*$^{-/-}$ mice treated as in **(a)**. **(f)** Absolute numbers of ILC1-like cells in in IL-12+IL-18 treated mice having received i.p injections of α-IFN-γ or control IgG. **(g)** Absolute numbers of IL-18Rα^{-} ILC2 (green), IL-18Rα^{+} ILC2 (yellow) and ILC1-like cells (blue) after intranasal administration of PBS (control), IL-12+IL-18, or IL-12+IL-18+IL-33. **(h)** Absolute numbers of ILC1-like cells after intranasal administration of PBS (control), neuromedin U (NMU), IL-12+IL-18, or IL-12+IL-18+NMU. In **(b, c, e-h),** each symbol represents an individual mouse. Statistical analysis was performed using Mann-Whitney (e, f) and two-way ANOVA **(b, c, g, and h)** tests (*, $p<0.05$; **, $P<0.01$; ***, $p<0.001$; ****, $p<0.0001$). Graphs depict data as mean (± s.e.m). Data are representative of three **(b-c, g)** and two **(d-f, h)** independent experiments.

Figure 4

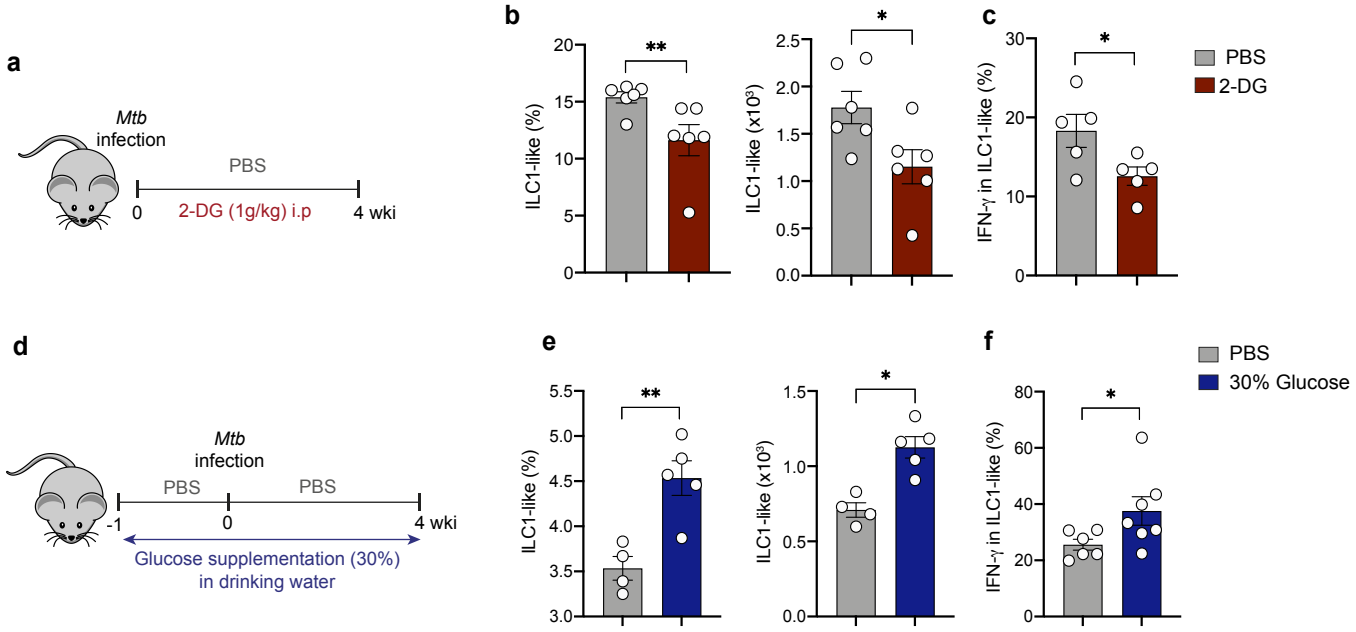
a
Mtb
infection
PBS
0
2-DG (1g/kg) i.p
4 wki
b
ILC1-like (%)
**
ILC1-like (x10³)
*
c
IFN-γ in ILC1-like (%)
*
PBS
2-DG
d
Mtb
infection
PBS
PBS
-1
0
4 wki
Glucose supplementation (30%)
in drinking water
e
ILC1-like (%)
**
ILC1-like (x10³)
*
f
IFN-γ in ILC1-like (%)
*
PBS
30% Glucose

Figure 4. Metabolic environment dictates ILC2 plasticity through glucose availability. (a) Scheme of the experimental model for *in vivo* treatment with 2-DG. **(b)** Percentages (left) and absolute numbers (right) of ILC1-like cells in *Rag2*$^{-/-}$ mice treated or not with 2-DG during *Mtb* infection. Measurements were performed at day 28 post-infection. **(c)** Percentages of IFNγ-producing cells among ILC1-like cells after *ex vivo* stimulation with PMA/ionomycin in the presence of brefeldin A for 4h from PBS *vs.* 2-DG treated mice. **(d)** Scheme of the experimental model for *in vivo* glucose supplementation in drinking water. **(e)** As in **(b)** except that mice treated with 30% glucose in their drinking water. **(f)** As in **(c)** except that mice were treated or not with 30% glucose in their drinking water. In **(b, c, e, f)**, each symbol represents an individual mouse and statistical analysis was performed using Mann-Whitney (*, $p<0.05$; **, $P<0.01$; ***, $p<0.001$; ****, $p<0.0001$). Graphs depict data as mean (± s.e.m) from three **(b, c)** or two **(e, f)** independent experiments.

Figure 5

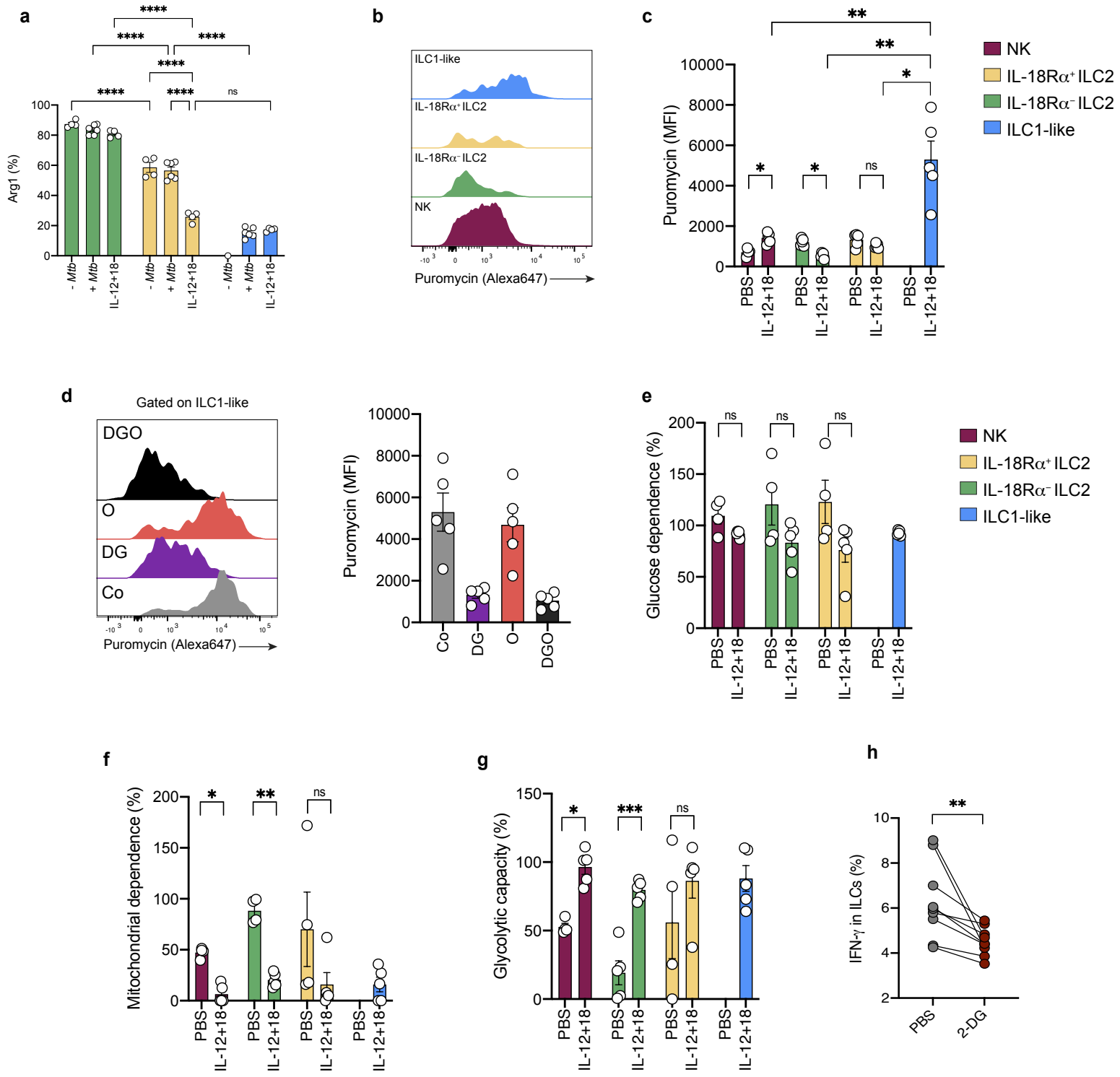
a
Arg1 (%)
- Mtb
+ Mtb
IL-12+18
ns
b
ILC1-like
IL-18Rα+ ILC2
IL-18Rα- ILC2
NK
Puromycin (Alexa647)
c
Puromycin (MFI)
PBS
IL-12+18
NK
IL-18Rα+ ILC2
IL-18Rα- ILC2
ILC1-like
d
Gated on ILC1-like
DGO
O
DG
Co
Puromycin (Alexa647)
Puromycin (MFI)
e
Glucose dependence (%)
f
Mitochondrial dependence (%)
g
Glycolytic capacity (%)
h
IFN-γ in ILCs (%)
2-DG

Figure 5. ILC1-like cells display a glycolytic dependence. (a) Percentages of Arg1$^+$ cells among IL-18Rα^- ILC2 (green), IL-18Rα^+ ILC2 (yellow), and ILC1-like cells (blue) defined at steady state (- *Mtb*), upon *Mtb* infection (+ *Mtb*) or intranasal administration of cytokines (IL-12+IL-18). **(b)** Representative histograms of puromycin staining in NK cells (violet), IL-18Rα ILC2$^-$ (green), IL-18Rα^+ ILC2 (yellow), and ILC1-like cells (blue) in IL-12+IL-18 treated mice. **(c)** Expression of puromycin (MFI) in NK cells (violet), IL-18Rα^- ILC2 (green), IL-18Rα^+ ILC2 (yellow), and ILC1-like cells (blue) in PBS *vs.* IL-12+IL-18 treated mice. **(d)** Representative histograms of puromycin staining (left) and quantification (MFI, right) in ILC1-like cells from IL-12+IL-18 treated mice after incubation with various metabolic inhibitors (Co, control; DG, 2-Deoxyglycose; O, oligomycin; DGO, 2-Deoxyglucose + Oligomycin). **(e-g)** Percentage of glucose dependence **(e)**, mitochondrial dependence **(f)**, and glycolytic capacity **(g)** in NK (violet), IL-18Rα^- ILC2 (green), IL-18Rα^+ ILC2 (yellow), and ILC1-like cells (blue) in PBS *vs.* IL-12+IL-18 treated mice. **(h)** Expression of IFN-γ in total ILCs after *ex vivo* stimulation with IL-12+IL-18 in the presence or absence of 2-DG. In **(a-h)**, graphs depict data as mean (± s.e.m) from two independent experiments, each symbol represents an individual mouse. Statistical analysis was performed using two-way ANOVA **(a, c, e, f, g)** or Wilcoxon **(h)** test (*, $p<0.05$; **, $P<0.01$; ***, $p<0.001$; ****, $p<0.0001$).

Figure 6

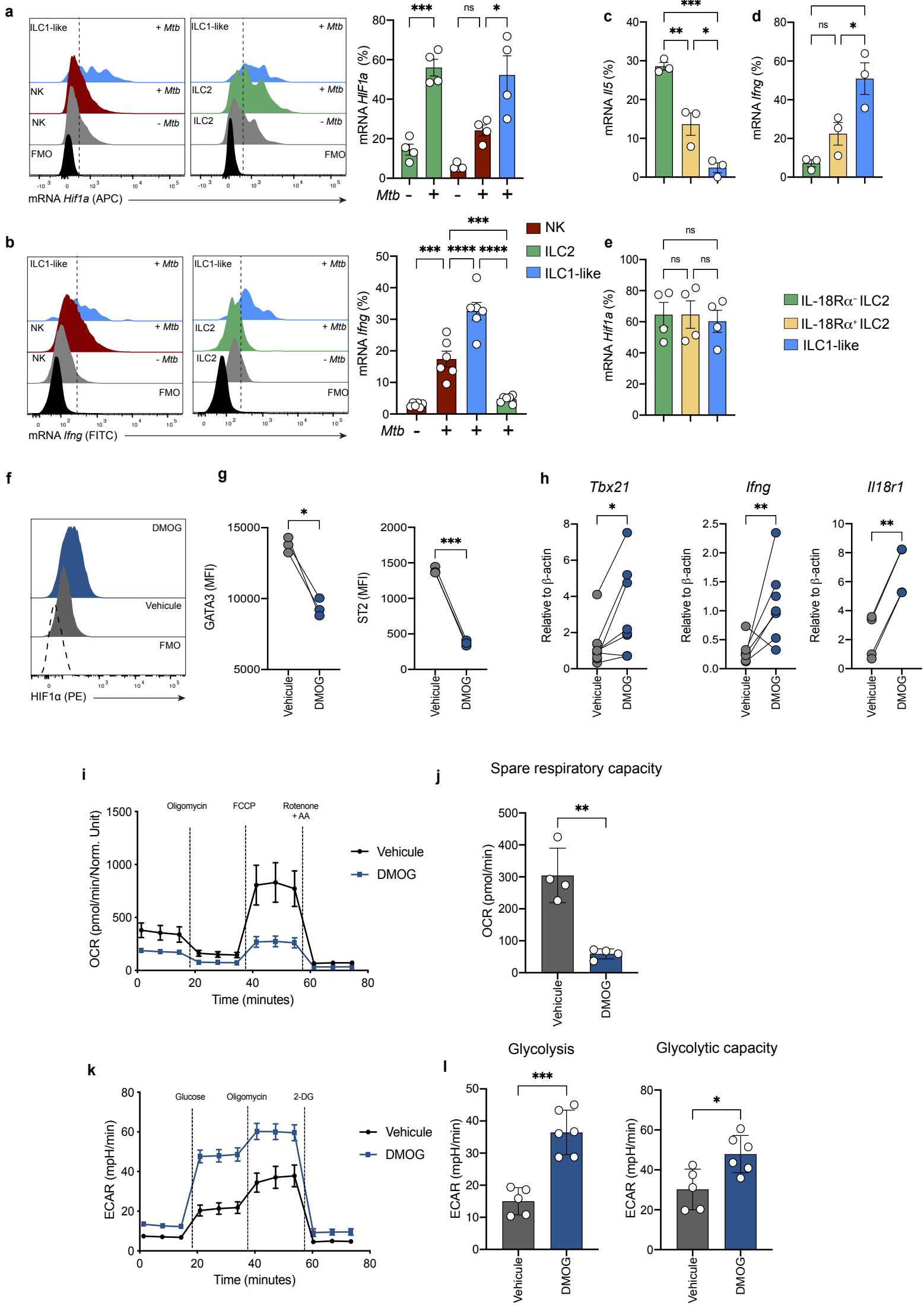
a
ILC1-like
+ Mtb
NK
+ Mtb
NK
- Mtb
FMO
ILC2
mRNA Hif1a (APC)
mRNA Hif1a (%)
Mtb
b
mRNA Ifng (FITC)
mRNA Ifng (%)
NK
ILC2
ILC1-like
c
mRNA Il5 (%)
d
mRNA Ifng (%)
e
mRNA Hif1a (%)
IL-18Rα⁻ ILC2
IL-18Rα⁺ ILC2
ILC1-like
f
DMOG
Vehicule
FMO
HIF1α (PE)
g
GATA3 (MFI)
ST2 (MFI)
Vehicule
DMOG
h
Tbx21
Ifng
Il18r1
Relative to β-actin
i
Oligomycin
FCCP
Rotenone + AA
OCR (pmol/min/Norm. Unit)
Time (minutes)
j
Spare respiratory capacity
OCR (pmol/min)
k
Glucose
Oligomycin
2-DG
ECAR (mpH/min)
l
Glycolysis
Glycolytic capacity

Figure 6. Metabolic reprogramming involving HIF1α controls ILC2 plasticity. (a) Representative histograms (left) and quantification (right) of *Hif1a* mRNA expression *via* prime-flow on NK cells (left) and ILC2 (middle) compared to ILC1-like cells in non-infected *vs. Mtb*-infected *Rag2*$^{-/-}$ mice (28 dpi). The dot line represents the positivity according to the fluorescence minus one (FMO). **(b)** As in **(a)** but for *Ifng* mRNA expression. **(c-e)** Percentages of the indicated IL-18Rα^{-} ILC2 (green), IL-18Rα^{+} ILC2 (yellow) and ILC1-like (blue) populations expressing *Il5* **(c)**, *Ifng* **(d)**, *Hif1a* **(e)** mRNA in *Mtb*-infected *Rag2*$^{-/-}$ mice (28 dpi). **(f)** Histograms showing HIF1α protein expression in ILC2 cultured in the absence (vehicle, grey) or presence of DMOG (blue). The dot line represents FMO for HIF1α detection. **(g)** Quantitative analysis of the intensity of GATA3 (left) and ST2 (right) expression in ILC2 cultured in the absence (vehicle) or presence of DMOG. **(h)** as in **(g)** except that the expression of *Tbx21*, *Ifng* and *Il18ra1* mRNA was analyzed by RT-qPCR. **(i, j)** Seahorse analysis of mitochondrial respiration (i) with quantification of spare respiratory capacity (j) in ILC2 cultured in the presence or absence of DMOG. **(k, l)** Seahorse analysis of glycolytic stress test (k) with quantitation of glycolysis and glycolytic capacity (**l**) of ILC2 cultured in the presence or absence of DMOG. Each symbol in **(a-e, g, h, j, and l)** represents an individual mouse. Statistical analysis was performed using two-ANOVA **(a-e),** and paired t test **(g-l)** (*, $p<0.05$; **, $P<0.01$; ***, $p<0.001$; ****, $p<0.0001$). Graphs depict data as mean (± s.e.m). Data are representative of three **(f)**, two **(a-e, g, i-l)**, a pool of three **(h)** independent experiments.

Figure 7

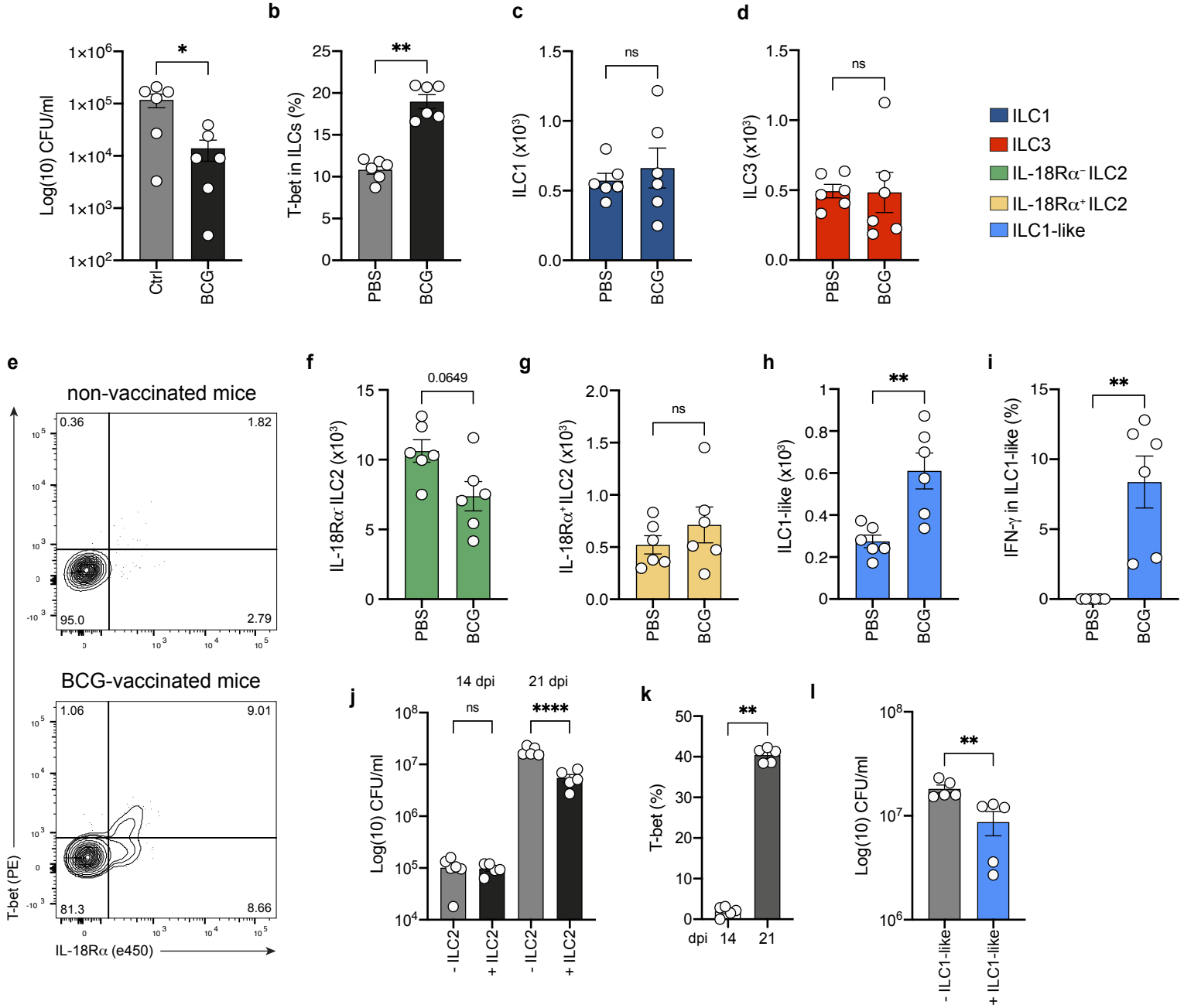
a
Log(10) CFU/ml
1×10^6
1×10^5
1×10^4
1×10^3
1×10^2
*
Ctrl
BCG
b
T-bet in ILCs (%)
25
20
15
10
5
0
**
PBS
BCG
c
ILC1 (x10^3)
1.5
1.0
0.5
0.0
ns
PBS
BCG
d
ILC3 (x10^3)
1.5
1.0
0.5
0.0
ns
PBS
BCG
ILC1
ILC3
IL-18Rα⁻ ILC2
IL-18Rα⁺ ILC2
ILC1-like
e
non-vaccinated mice
0.36
1.82
95.0
2.79
BCG-vaccinated mice
1.06
9.01
81.3
8.66
T-bet (PE)
IL-18Rα (e450)
f
IL-18Rα⁻ ILC2 (x10^3)
15
10
5
0
0.0649
PBS
BCG
g
IL-18Rα⁺ ILC2 (x10^3)
2.0
1.5
1.0
0.5
0.0
ns
PBS
BCG
h
ILC1-like (x10^3)
1
0.8
0.6
0.4
0.2
0
**
PBS
BCG
i
IFN-γ in ILC1-like (%)
15
10
5
0
**
PBS
BCG
j
14 dpi
21 dpi
Log(10) CFU/ml
10^8
10^7
10^6
10^5
10^4
ns
****
- ILC2
+ ILC2
- ILC2
+ ILC2
k
T-bet (%)
50
40
30
20
10
0
**
dpi 14
21
l
Log(10) CFU/ml
10^8
10^7
10^6
**
- ILC1-like
+ ILC1-like

Figure 7. ILC1-like cells confer protection against *Mtb*. (a) Mycobacterial loads at day 14 post-infection in C57BL/6 mice vaccinated or not (PBS) with $1x10^5$ BCG via the intranasal route 60 days prior *Mtb* infection. **(b)** Percentages of total lung ILC expressing T-bet. **(c-d)** Absolute numbers of ILC1 **(c)** andILC3 **(d)** at day 14 post-infection in C57BL/6 mice vaccinated or not (PBS) with $1x10^5$ BCG via the intranasal route 60 days prior *Mtb* infection. **(e)** Representative dot-plots of T-bet and IL18Rα expression in *Mtb*-infected non-vaccinated (top) *vs.* BCG-vaccinated (bottom) mice at day 14 post-infection. **(f-h)** Absolute numbers of IL-18Rα^- ILC2 **(f)**, IL-18Rα^+ ILC2 **(g),** and ILC1-like cells **(h)** at day 14 post-infection in C57BL/6 mice vaccinated or not (PBS) with $1x10^5$ BCG via the intranasal route 60 days prior *Mtb* infection. **(i)** Percentage of IFN-γ^+ cells among ILC1-like cells in *Mtb*-infected unvaccinated *vs.* vaccinated mice after *ex vivo* stimulation with PMA/ionomycin in the presence of brefeldin A for 4h. **(j)** Mycobacterial loads at day 14 and 21 post-infection in *Rag2*$^{-/-}$ *Il2rg*$^{-/-}$ mice having received (+ILC2) or not (-ILC2) an adoptive transfer of sorted ILC2 cells one day before *Mtb* infection. **(k)** In the model presented in **(j)**, T-bet expression was analyzed in lung ILCs 14- or 21-days post *Mtb* infection. **(l)** Bacterial loads at day 21 post-infection in *Rag2*$^{-/-}$*Il2rg*$^{-/-}$ mice having received (+ILC1-like) or not (-ILC1like) an adoptive transfer of ILC1-like cells from IL-12+IL-18+IL-33 treated *Rag2*$^{-/-}$ mice one day before *Mtb* infection. Each symbol in **(a-d, f-l)** represents an individual mouse. Statistical analysis was performed using Mann-Whitney test **(a-d, f-i, k, l)** and two-way ANOVA **(j)** (*, $p<0.05$; **, $P<0.01$; ***, $p<0.001$; ****, $p<0.0001$). Graphs depict data as mean (± s.e.m). Data are representative of one **(a-i),** three **(j, k)** and two **(l)** independent experiments.